Multiscale Variability of the Atmospheric Mixed Layer over the Western Pacific Warm Pool

RICHARD H. JOHNSON, PAUL E. CIESIELSKI, AND JENNIFER A. COTTURONE

Department of Atmospheric Science, Colorado State University, Fort Collins, Colorado

(Manuscript received 13 September 2000, in final form 2 March 2001)

ABSTRACT

Sounding data from Tropical Ocean Global Atmosphere Coupled Ocean–Atmosphere Response Experiment (TOGA COARE) have provided a first opportunity to document the variability of the atmospheric mixed layer over the western Pacific warm pool on timescales ranging from diurnal to intraseasonal. Six-hourly sounding data from four sites—the atoll Kapingamarangi and R/Vs *Moana Wave*, *Shiyan 3*, and *Xiangyanghong 5*—are used to determine the mixed layer depth and its thermodynamic properties. Almost three-quarters of the soundings at these four sites exhibited well-mixed structures: nearly constant profiles of potential temperature and specific humidity capped by a ~150-m-deep entrainment zone. The majority of the remaining soundings were modified by precipitation and their associated downdrafts. It is estimated that approximately 40%–50% of the total soundings in COARE were influenced by precipitation downdrafts.

The mean mixed layer depth at the four sites was 512 m with large variations on multiple timescales. Mean depths decreased across the warm pool from west to east, consistent with the west-to-east increase in precipitation averaged over the 4-month Intensive Observing Period. Significant modulation of the mixed layer occurred on the timescale of the Madden–Julian oscillation (MJO): the mean depth was 562 m during the undisturbed, light-wind period prior to the strong westerly wind burst (WWB) associated with the December MJO; it decreased to 466 m during the heavy-rain period of the WWB, reflecting numerous, recovering precipitation downdraft wakes; and then increased to 629 m during the late stages of the WWB when precipitation had ended. Dry intrusions over the warm pool caused the mixed layer to deepen at times to 800 m and more. Since the surface buoyancy flux typically did not increase at these times, the deepening is linked to a suppression of shallow cumulus clouds by the dry air (reduced between-cloud subsidence) as well as a general reduction in the overall shower activity and associated precipitation downdrafts. Dry intrusions also acted to enhance radiative cooling in the mixed layer.

A diurnal cycle in the mixed layer depth was observed, with maximum amplitude in undisturbed (mostly clear), light-wind conditions. The mixed layer was deepest and warmest in the afternoon in direct response to 1) an afternoon peak in the surface buoyancy flux, which, in turn, arose from the large diurnal cycle in SST (up to 2°–3°C) on light-wind days, and 2) absorption of solar shortwave radiation. Thus, the atmospheric mixed layer over the warm pool during undisturbed conditions behaves like that over land, albeit with a weaker diurnal cycle amplitude, but sufficient to generate an afternoon maximum in shallow cumulus clouds and precipitation. This pattern is distinct from the typical early morning maximum in rainfall during disturbed conditions over tropical oceans. Diagnosis of the mixed layer net radiative cooling rate during light-wind conditions indicates a large diurnal range, from ~ -1.5 K day^{-1} at midday to nearly -3 K day^{-1} at night.

1. Introduction

The western Pacific warm pool is a site of highly variable and complex air–sea exchanges over a wide range of timescales—from minutes and hours (e.g., in response to showers), to the diurnal cycle, to weeks and months (in connection with intraseasonal oscillations), to years (e.g., due to El Niño–Southern Oscillation). Considering that the warm pool is a site of maximum rainfall in the Tropics, convection plays an important role in air–sea coupling in this region. Precipitation significantly modifies the upper-ocean mixed layer (Anderson et al. 1996), contributing to the production of a freshwater lens or ''barrier layer'' (Lukas and Lindstrom 1991), hypothesized to be an important factor in maintaining the high sea surface temperatures (SSTs) in the tropical western Pacific. The atmospheric boundary layer (typically, the lowest 0.5 km of the troposphere) is also modified by convection, principally through downdrafts that transport cool air toward the ocean surface. A lack of understanding of the coupling between the ocean and atmosphere over the western Pacific warm pool led to its selection as the site for the Tropical Ocean Global Atmosphere Coupled Ocean–Atmosphere Response Experiment (TOGA COARE) from November 1992 through February 1993 (Webster and Lukas 1992).

Corresponding author address: Richard H. Johnson, Department of Atmospheric Science, Colorado State University, Fort Collins, CO 80523.
E-mail: rhj@atmos.colostate.edu

a. Convective-scale to large-scale variability

Studies of the ocean mixed layer during COARE reveal significant variability on multiple timescales resulting from forcing by the diurnal cycle of solar heating, short-lived squalls and rainfall events, and week-long westerly wind bursts (e.g., Godfrey et al. 1998). These same forcing mechanisms have also been found to have a pronounced impact on the atmospheric mixed layer. Much attention has been given to observations of the modification and recovery of the atmospheric boundary layer following deep convection (Parsons et al. 1994; Raymond 1995; Young et al. 1995; Jorgensen et al. 1997; Williams et al. 1997; Kingsmill and Houze 1999). These studies have shown that organized deep convective systems in COARE frequently produced cool downdraft wakes, with temperature deficits up to 4° to 5°C and recovery times up to 12 h. These general properties of downdraft wakes over the warm pool resemble those observed over the eastern Atlantic during the GARP Atlantic Tropical Experiment (GATE) (Houze 1977; Zipser 1977; Fitzjarrald and Garstang 1981; Johnson and Nicholls 1983) despite the considerably higher SSTs in the western Pacific. Several studies have shown that the surface sensible and latent heat fluxes in COARE were markedly enhanced by mesoscale convective systems (Jabouille et al. 1996; Sun et al. 1996; Geldmeier and Barnes 1997; Saxen and Rutledge 1998). Esbensen and McPhaden (1996) showed that such enhancement of monthly averaged surface evaporation approaches 30% of the total surface evaporation, suggesting this effect should be included in surface flux parameterizations for global models (Redelsperger et al. 2000).

In addition to effects of precipitation, recent studies have shown that dry intrusions over the warm pool can have a significant impact on the atmospheric boundary layer (Numaguti et al. 1995; Parsons et al. 2000). Maximum drying associated with dry intrusions is typically observed in the lower troposphere (~600–800 hPa), but in some instances the dry air is entrained downward to produce deep, dry mixed layers (Parsons et al. 2000). These authors note that the dry intrusions tend to be associated with temperature inversions, likely induced by radiative effects (Mapes and Zuidema 1996), which can increase convective inhibition (CIN) and suppress convection for a number of days. Zhang and Chou (1999) also show how dry intrusions in the lower troposphere can enhance the infrared cooling rate in the mixed layer.

Studies of the mean characteristics of the COARE atmospheric boundary layer (ABL), including both disturbed and undisturbed conditions, are rather limited. Serra et al. (1997) used *Electra* aircraft data from 25 flights over a range of atmospheric conditions to document the mean and turbulent structure of the COARE atmospheric boundary layer. For undisturbed conditions, they found a mean mixed layer height of 600 m having nearly constant potential temperature θ but decreasing specific humidity q with height. Mean profiles for disturbed conditions exhibited stable stratification throughout the boundary layer, reflecting the frequent occurrence of stable layers and recovering shallow mixed layers arising from convective downdrafts. LeMone et al. (1998) presented mean boundary-layer thermodynamic profiles of the undisturbed environment of convection using 19 COARE aircraft soundings and noted that the structures of θ and q resembled those of the undisturbed trades.

One of the purposes of this paper is to add to the knowledge of the mean structure and properties of the COARE ABL and its variability over a wide range of timescales using six-hourly sounding data from various sites in the COARE domain. In our analyses we incorporate recent corrections made to the humidity data from Vaisala H-Humicap sensors (Guichard et al. 2000). The mean characteristics will be compared to those from COARE aircraft measurements and those from other tropical marine environments (e.g., GATE). In addition, the variation of the properties of the ABL on the 30–60-day timescale of the Madden–Julian oscillation (MJO; Madden and Julian 1971) will be examined. Since there is mounting evidence that the MJO is a coupled atmosphere–ocean phenomenon (Flatau et al. 1997; Hendon and Glick 1997; Woolnough et al. 2000) and the mixed layer is the medium through which the free atmosphere and ocean are coupled, it is important to document the properties and evolution of the mixed layer on MJO timescales.

b. Diurnal variability

A remarkable aspect of the western Pacific warm pool is the frequent occurrence of quiescent periods, with wind speeds less than 1–2 m s^{-1}, along with an accompanying large diurnal range in the SST, at times up to 2°–3°C (Halpern and Reed 1976; Stramma et al. 1986; Lukas 1991; Flament et al. 1994; Weller and Anderson 1996). The amplitude of the diurnal cycle is greatest under calm, clear-sky conditions. However, the afternoon warming of the ocean surface can lead to increased cloudiness, which in turn can damp the diurnal SST cycle (Lukas 1991; Chen and Houze 1997; Webster et al. 1996). Ship-based radar data from TOGA COARE reveal an afternoon maximum in shallow, precipitating convective cells during undisturbed periods (Rickenbach and Rutledge 1997; Sui et al. 1997a; Sui et al. 1998), indicating that the effects of the surface heating are being communicated to the lower troposphere. Further evidence can be seen in ceilometer data reported by White et al. (1995), who found a significant diurnal variation in the COARE-mean cloud base height, with a prominent late-afternoon (1730 L) maximum.

Several studies have examined the impact of clouds, precipitation, and the diurnal cycle on SST and the upper ocean in the warm pool region (Lukas and Lindstrom 1991; Webster et al. 1996; Soloviev and Lukas 1997; Sui

et al. 1997b). In contrast, the diurnal behavior of the atmospheric boundary layer has not yet been extensively investigated, due in part to the lack of direct observations. Two exceptions are the studies of Serra et al. (1997) and Parsons et al. (2000). Serra et al. examined the variation of the mixed layer for the daylight portion of the diurnal cycle using aircraft data. They found that during undisturbed, light-wind conditions, the lowest portion of the boundary layer was stably stratified at and just after sunrise due to nocturnal cooling of the ocean surface. By afternoon, a well-mixed profile of q was observed, the θ profile became slightly unstable due to surface heating, and the boundary-layer winds increased. Parsons et al. (2000) showed evidence of a diurnal variation in the boundary-layer virtual temperature of 0.5°–1.5°C. They argued that during undisturbed conditions with dry air above the boundary layer, a combination of the diurnal cycle of SST and absorption of shortwave radiation (primarily by water vapor) reduced CIN in the afternoon, thereby leading to a late afternoon, early evening maximum in shallow convection.

In this study 6-hourly COARE sounding data are used to examine the diurnal variation of the atmospheric mixed layer over the warm pool. While a 6-h frequency is not adequate to fully resolve the diurnal cycle, the data have the advantage of representing a nearly continuous and distributed measurement of boundary-layer properties throughout the COARE Intensive Observing Period (IOP) over the central COARE domain. They also represent an extension of the aircraft results of Serra et al. (1997) into the nighttime hours. Also in this study, we incorporate the observed characteristics of the boundary layer into a simple mixed layer model to diagnose its radiative properties.

2. Data sources

a. Sounding sites and vertical resolution

During the TOGA COARE IOP (November 1992–February 1993), a network of sounding stations was established over the equatorial western Pacific. The innermost portion of the network was the Intensive Flux Array (IFA), with 4 day^{-1} soundings (Fig. 1). Instrumentation included National Center for Atmospheric Research (NCAR)–National Oceanic and Atmospheric Administration Integrated Sounding Systems (ISSs) consisting of 915-MHz wind profilers, acoustic sounders, omegasondes, and surface meteorological stations (Parsons et al. 1994). The sounding data used in this study are from four stations within the IFA shown in Fig. 1: the small atoll Kapingamarangi (ISS site; hereafter referred to as Kapinga), and R/Vs *Moana Wave*, *Shiyan 3* (ISS site; hereafter referred to as *Ship 3*), and *Xiangyanghong 5* (hereafter referred to as *Ship 5*).[1]

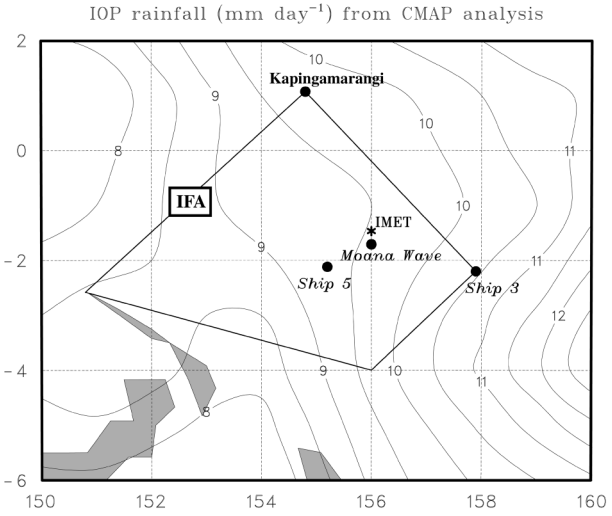

FIG. 1. Sounding sites (filled circles) within the TOGA COARE Intensive Flux Array (IFA) used in this study. Asterisk at 1°45′S, 156°E indicates the position of the IMET buoy described in the text. Also shown are contours of IOP-mean rainfall rate (mm day^{-1} with a contour interval of 0.5 mm day^{-1}) based on Xie and Arkin (1997) CMAP analysis.

These sites were selected because they represent open-ocean ABL conditions with minimal land effects. However, Kapinga does appear to have some land influence, as will be seen later. The wind data at Kapinga and *Ship 3* are based on a merger of each site's omegasonde wind observations and wind profiler data (Ciesielski et al. 1997). For omegasondes, the first wind data point above the surface was typically about 600 m and for the profilers the lowest altitudes of reliable winds were at 400 m for Kapinga and 700 m for *Ship 3*. Therefore, the resolution of winds in the boundary layer is poor and in many cases the mixed layer wind profiles are simply a linear interpolation between the surface wind and the lowest sonde wind.

Also included in Fig. 1 is the IOP-mean rainfall distribution based on the Climate Prediction Center Merged Analysis of Precipitation (CMAP; Xie and Arkin 1997). It depicts generally increasing IOP-mean rainfall amounts from west to east across the IFA. Thus, we expect (and later report) a progressively increasing disruption of the boundary layer by convection from *Ship 5* in the west to *Ship 3* in the east.

Two vertical resolutions are available from the COARE sounding archive (Loehrer et al. 1996): 10-s data and 5-hPa data (interpolated linearly in log pressure from the 10-s data). We have used the 5-hPa dataset in our study to locate mixed layer depths in 5-hPa bins. Since the ascent rate of the balloons is ~5 m s^{-1} in the lower troposphere where 10 m ≈ 1 hPa, the two datasets represent roughly the same resolution (~50 m) in the boundary layer. Thus, the depth of the mixed layer, identified in this study (using a procedure to be described later) by sharp changes in stability and moisture gra-

[1] The location of *Ship 5* in Fig. 1 represents its average position for its last two cruises (dates in Table 1). High-resolution data were unavailable for the first cruise (5–30 November), so analyses for *Ship 5* were performed only for cruises 2 and 3.

dients at its top, can be determined within 50 m. The entrainment zone or inversion atop the mixed layer, typically ~100–200 m deep over tropical oceans (Malkus 1958; Augstein et al. 1974; LeMone and Pennell 1976), is marginally resolved with this dataset.

b. Corrections to humidity data

Following the field phase of TOGA COARE, a variety of errors in the sounding humidity data were identified at many of the sites (Loehrer et al. 1996; Zipser and Johnson 1998; Lucas and Zipser 2000). Although multiple humidity sensors were employed in COARE, those used at the four sites in this study were Vaisala H-Humicap sensors. Recently, a revised sounding dataset has been released by NCAR that incorporates corrections to the H-sensor data (E. Miller 2000, personal communication). For the sites used is this study, only a small proportion (<4%) of the soundings were not corrected.

The corrections are of several types. First, there is a correction for a ~5% dry bias (at high relative humidities) of the Vaisala H-Humicap humidity sensor owing to a contamination of the dielectric polymer by aging sensor packaging material. Second, at Kapinga corrections were made to the lowest levels of the sounding data due to errors introduced by launching of sondes from an air-conditioned van. Finally, errors in the near-surface data due to sensor-arm heating in the daytime and radiative cooling at night were corrected using independently measured surface relative humidities. Details of the correction procedures can be found in Guichard et al. (2000) and references therein.

The corrected humidity data have been used in the construction of the vertical profiles presented in this study. However, determination of the mixed layer depths (using a procedure described in section 3) has been based on an earlier version of the sounding data (Loehrer et al. 1996) that did not incorporate the humidity corrections. Inspection of the vertical profiles for the revised dataset shows that the determination of mixed layer depths is not altered by the new data since the procedure relies on the *vertical gradients* of temperature and moisture, which are not materially affected by the moisture corrections that have been applied.

c. Other data sources

Although not colocated with the sounding sites, the Woods Hole Oceanographic Institution Improved Meteorology (IMET) buoy at 1°45′S, 156°E (location shown in Fig. 1) is used to provide background information on surface sensible and latent heat fluxes (data from Weller and Anderson 1996). In addition, satellite rainfall estimates are obtained from two sources: 1) the CMAP of Xie and Arkin (1997), and 2) the mixed rainfall algorithm of Curry et al. (1999). CMAP data, which consist of pentad values, are used to depict the large-scale mean rainfall distribution, whereas the data of Curry et al. available at 3-h intervals are used for analyses of higher temporal variability. Tipping bucket rain gauge data at Kapinga were also used to provide high temporal resolution of rainfall at that site. Ceilometer data from White et al. (1995) are used to determine the diurnal cycle of fractional cloudiness at *Moana Wave.* The maximum vertical range of the ceilometer is 3.5 km, so for the undisturbed period for which the ceilometer data will be used, only shallow clouds (mostly cumulus) are observed. As discussed by White et al. there are limitations in interpreting the magnitudes of fractional cloudiness from ceilometer data; however, in this study only relative values are emphasized in connection with the diurnal cycle of shallow cumulus.

3. Procedure for determining mixed layer depth

Observations from the Carribean and Atlantic (Bunker et al. 1949; Malkus 1958; Augstein et al. 1974; Pennell and LeMone 1974; LeMone and Pennell 1976; Brümmer 1978; Fitzjarrald and Garstang 1981) and the eastern Pacific (Firestone and Albrecht 1986; Bond 1992; Yin and Albrecht 2000) show that within the tropical atmospheric mixed layer the potential temperature is approximately constant with height. Specific humidity profiles in these studies range from well-mixed structures to ones where q gradually decreases with height (by 0.5–1 g kg^{-1}) through the depth of the mixed layer. The latter profiles have been attributed to dry-air entrainment into the mixed layer, as evidenced by large specific humidity variances reported near mixed layer top (e.g., Nicholls and LeMone 1980). The mixed layer is capped by a transition layer (or entrainment zone) ~100–200 m deep characterized by a sharp increase in stability and decrease in specific humidity. Recent aircraft soundings from COARE show similar structure and properties of the mixed layer over the tropical western Pacific (Serra et al. 1997; LeMone et al. 1998).

In this study a subjective technique has been used to identify mixed-layer tops at the four sounding sites. The technique utilizes information in both the θ and q profiles. Specifically, the mixed layer top z_i is identified as the level at which θ exhibits an abrupt increase with height (following a nearly constant value below) and q exhibits a sharp decrease with height (following a gradual decrease or constant value below). If evidence does not exist for these structures in *both* the θ and q profiles, then a z_i is not assigned to that sounding. The top of the entrainment zone was not determined in this analysis; however, it does appear in depictions of scaled boundary-layer thermodynamic profiles to be presented later.

Shown in Fig. 2 are examples of soundings to which this procedure was applied at *Moana Wave* and Kapinga for three different weather regimes: a light-wind period, a westerly wind burst period, and a convective wake. In these cases, the mixed layer top z_i is well defined in

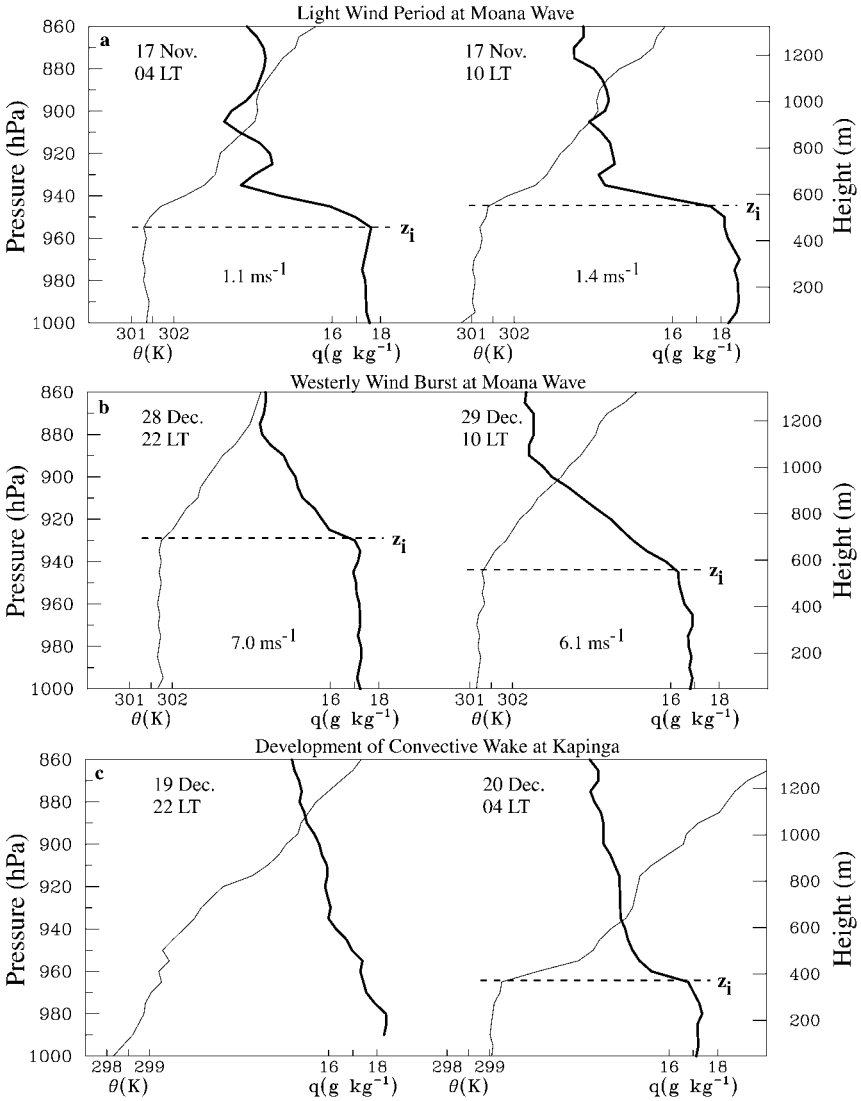

FIG. 2. Examples of soundings (potential temperature θ in thin solid lines and specific humidity q in heavy solid lines) depicting the identification of the mixed layer top z_i (horizontal dashed line) for three different weather regimes in TOGA COARE: (a) a light-wind period at *Moana Wave* at 0400 and 1000 LST 17 Nov 1992, (b) during a westerly wind burst at *Moana Wave* at 2200 LST 28 Dec and 1000 LST 29 Dec 1992, and (c) during the development of a convective wake at Kapinga at 2200 LST 19 Dec and 0400 LST 20 Dec 1992. The wind speeds shown in (a) and (b) indicate the mixed layer mean value for these soundings.

both the θ and q profiles. Sharp drying above z_i can be seen for the light-wind and convective wake cases. These results typify those observed throughout COARE: mixed layers were generally about 500–600 m deep during light-wind periods (Fig. 2a), deeper during strong winds (Fig. 2b), and shallow in recovering convective wakes (Fig. 2c). The sounding at 2200 LST in Fig. 2c is an example of a case where a mixed layer could not be identified. During undisturbed and the latter part of westerly wind burst periods, the mixed layers in COARE were frequently topped by cumulus layers (Fig. 3), resembling trade wind cumulus layers (e.g., Augstein et al. 1974; Johnson and Lin 1997). Increases in stability and drying were frequently seen atop the cumulus layers near 800 hPa or 2 km, as seen in Fig. 3 for Kapinga.

Using this subjective method, an average of 72% of the soundings at the four sites revealed detectable mixed layers (Table 1), with similar percentages (69%–74%) at each site. The majority of the remaining soundings were influenced by precipitation and their associated downdrafts. These results are consistent with the findings of Fitzjarrald and Garstang (1981), who used the Boundary Layer Instrumentation System in GATE to objectively determine mixed layer tops by fitting each

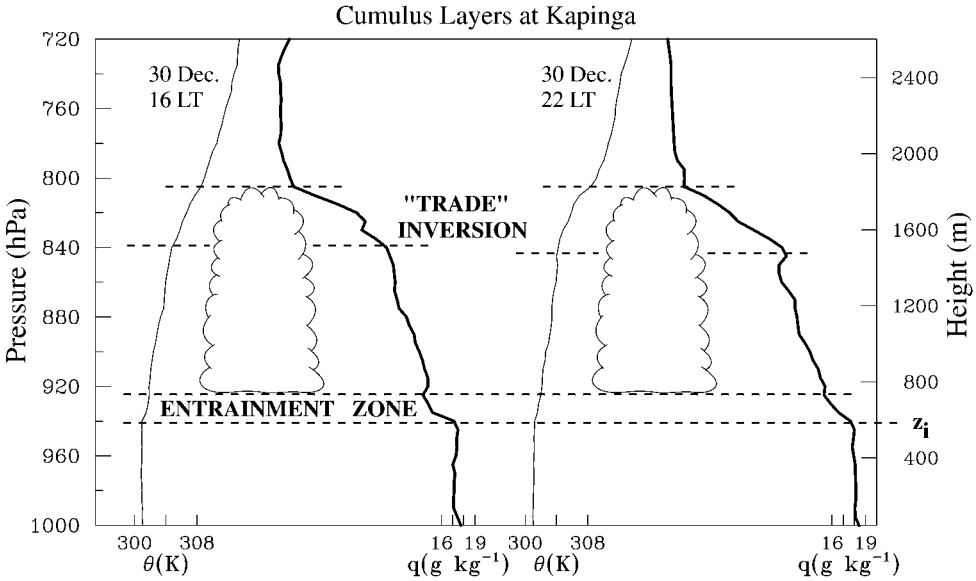

FIG. 3. Example of soundings (potential temperature θ in thin solid lines and specific humidity q in heavy solid lines) at Kapinga at 1600 and 2200 LST 30 Dec 1992 depicting a period when the mixed layer was topped with a shallow cumulus layer. Also indicated are the entrainment zone atop the mixed layer, and a ''trade-type'' inversion layer between 840 and 800 hPa.

profile with a slightly smoothed cubic spline. Of the total 703 GATE profiles, 559 (79.5%) showed a mixed layer structure based on their objective method.

4. Mean properties of the mixed layer

The IOP-mean properties of the mixed layers for the four sites are given in Table 2. The overall mean z_i for the four sites is 512 m. This value is slightly greater than Fitzjarrald and Garstang's (1981) GATE mean of 424 m for a similarly large data sample and for a region (eastern Atlantic) with both disturbed and undisturbed conditions. It is comparable to the ~500-m mean z_i reported by Bond (1992) for the equatorial eastern Pacific. The COARE mean is somewhat lower than the ~600-m mean z_i's reported for the undisturbed trades of the Carribean and western and central Atlantic by Bunker et al. (1949), Malkus (1958), Augstein et al. (1974), Pennell and LeMone (1974), and LeMone and Pennell (1976). This difference can be explained by the fact that the COARE mean in Table 2 includes both undisturbed conditions and disturbed conditions, the latter being characterized by shallow mixed layers in recovering downdraft wakes. As will be seen later, the undisturbed COARE mixed layer depths compare well with those reported in the undisturbed trades of the Carribean and Atlantic.

TABLE 1. Frequency of mixed layers for COARE IOP.

Station (Obs periods, month/day)	Total soundings	No. with mixed layers	Percent
Ship 5 (12/15–1/09) (1/24–2/19)	207	142	69
Kapinga (entire IOP)	475	351	74
Moana Wave (11/11–12/03) (12/18–1/12) (1/28–2/14)	255	189	74
Ship 3 (11/10–12/12) (12/18–1/23) (1/31–2/18)	346	244	71
Total/Mean	1283	926	72

The large standard deviation (155 m) and range of z_i (116–961 m) (Table 2) reflect the existence of numerous processes affecting the mixed layer depth over the warm pool: from showers, squalls, and westerly wind bursts during disturbed periods; to isolated showers and mesoscale circulations such as horizontal convective rolls and open-cell convection during undisturbed periods; to the diurnal cycle and dry-air intrusions throughout the IOP. Fitzjarrald and Garstang (1981) report a similarly large standard deviation of z_i (160 m) during GATE.

The mean mixed layer depths generally decrease from west to east, ranging from a high of 553 m at *Ship 5* to a low of 491 m at *Ship 3* (Table 2). This variation is consistent with the west-to-east increase in the IOP-mean rainfall rates (Fig. 1) corresponding to heavier rainfall events and/or a higher frequency of shallow, recovering precipitation downdraft wakes toward the east. This relationship is not perfect ($\overline{z}_i$ at Kapinga is greater than at *Moana Wave* despite the IOP-mean rain rate being slightly greater at the former), but the periods

TABLE 2. IOP-mean mixed layer statistics. Numbers in last two columns based on soundings with corrected humidity data only; other numbers based on all soundings.

Station	No.	$\bar{z}_i$ (m)	σ (m)	$z_{i\max}$ (m)	$z_{i\min}$ (m)	Skewness	LCL (m)	LCL $-$ $\bar{z}_i$ (m)
Ship 5	142	553	146	950	205	0.1	723	170
Kapinga	351	518	155	961	196	0.1	687	169
Moana Wave	189	501	155	864	180	0.2	741	240
Ship 3	244	491	159	961	116	−0.2	662	171
Total/Mean	926	512	155	961	116	0.1	696	183

of observations are not the same for all sites (Table 1). Moreover, despite being a fairly small atoll, Kapinga may not be representative of open-ocean conditions both due to direct land heating/cooling effects and modification of the sea state in shallow lagoons.

Histograms of the mixed layer depths in 5-hPa bins for the four sites are shown in Fig. 4. Based on a chi-square test, the distributions are normal (at the 0.05 significance level), except at *Ship 3*. *Ship 3* exhibits a negative skewness, whereas there is a slight positive skewness for the other sites. The positive skewness is related to the existence of a lower boundary (there is no upper boundary to restrict the development of deep mixed layers, although there are natural processes that limit growth). However, in the case of *Ship 3*, which experiences the greatest precipitation, there is a skewness toward smaller depths and departure from a normal distribution due to the existence of more numerous shallow, recovering mixed layers.

Assuming that soundings with $z_i < 400$ m ($\sim$ one-third of the total according to Fig. 4) were impacted by precipitation and many of the 28% nonmixed layer soundings were similarly affected, it is estimated that 40%–50% of the total soundings in COARE were influenced by precipitation downdrafts. This range is similar to the 30%–50% estimates reported for GATE (Gaynor and Ropelewski 1979; Fitzjarrald and Garstang 1981).

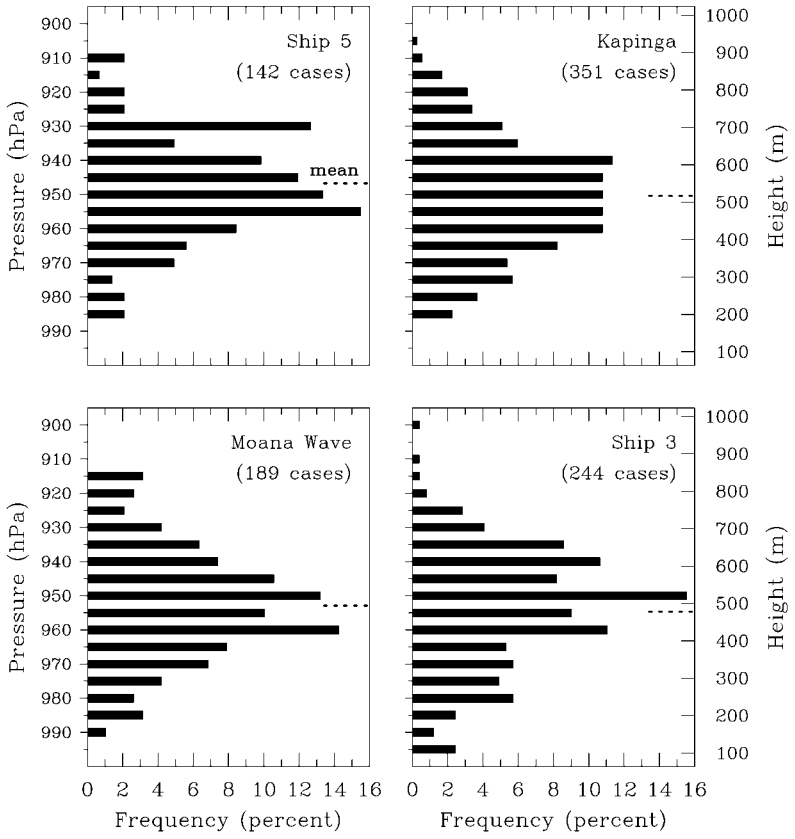

FIG. 4. Histograms for four sounding sites showing the frequency of occurrence (percent) that a mixed layer top falls within a 5-hPa bin. Number of cases in which a mixed layer was identified are indicated in parentheses. The mean mixed layer top for each site is indicated with a short dashed line along the right axis of each panel.

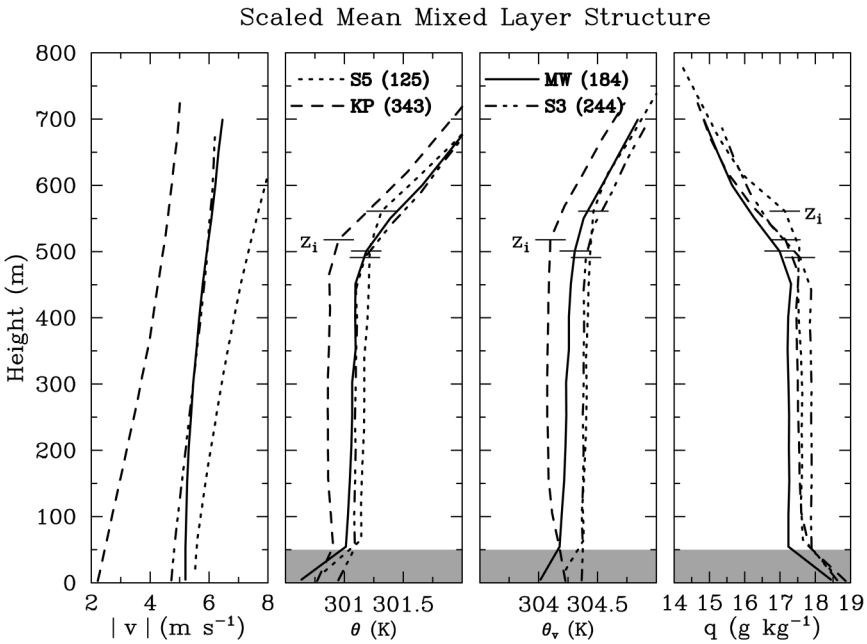

FIG. 5. Scaled mean mixed layer profiles of wind speed (left panel), potential temperature (left-center panel), virtual potential temperature (right-center panel), and specific humidity (right panel) for four sites constructed using humidity-corrected soundings with number of sondes used indicated in parentheses. Here S5, KP, MW, and S3 refer to *Ship 5*, Kapingamarangi, *Moana Wave*, and *Ship 3*, respectively. Mean values of the mixed layer top are indicated with short solid lines intersecting the θ, θ_v, and q curves. Shaded regions in the lowest 50 m of panels indicates questionable thermodynamic data in this layer.

To create mean profiles that preserve boundary-layer structures, kinematic and thermodynamic variables for each of the mixed layer soundings have been scaled according to mixed layer depth. Scaled-mean profiles of wind speed, θ, virtual potential temperature θ_v, and q for the four sites are shown in Fig. 5. Only humidity-corrected sondes were used in the construction of these plots. The profiles are in good agreement, except for Kapinga where the winds were 2–3 m s^{-1} lighter and θ was ~0.25 K cooler than the average for the other sites. The cooler conditions at Kapinga may reflect the slight effects of boreal winter at this northernmost site. From ~50 m above the surface to ~50 m below z_i, nearly well-mixed profiles of θ, θ_v, and q are evident. Slightly stable or near-neutral conditions are seen in the θ_v profiles near the surface. In section 7 it is shown that these conditions occur primarily at night. In the case of the ships, while some instances of slight stability at night may be real (Serra et al. 1997) they may also reflect some contamination from the ships' structures or an inconsistency between the surface observations (from measurements on the ships' masts) and the lowest points in the sounding data. Tower measurements aboard the *Moana Wave* indicate near-neutral or slightly unstable conditions near the surface over the ocean 99% of the time (C. Fairall 2000, personal communication). Therefore, we regard the lowest 50 m of the thermodynamic profiles as questionable and thus shade them in Fig. 5. For Kapinga, the surface meteorological station failed from late-November until early January, so near-surface values there are also untrustworthy.

The mixed layer mean values of specific humidity[2] in Fig. 5, ranging from 17.2 to 17.9 g kg^{-1}, are in good agreement with the ~17–18 g kg^{-1} values reported by Serra et al. (1997) and LeMone et al. (1998) based on aircraft flights in undisturbed conditions. However, unlike the results in Fig. 5, the aircraft mean profiles show q decreasing with height, particularly in the upper half of the mixed layer. This structure arises from level-by-level averaging of the aircraft data without scaling with respect to the mixed layer depth. This effect can be seen in Fig. 6, which shows mean θ and q profiles constructed in this way for the 189 mixed layer soundings from *Moana Wave* along with standard deviations (profiles are similar for other sites).

Slight changes in the gradients of θ and q ~ 100–150 km above z_i (Fig. 5) indicate the top of the entrainment zone. This height range is in reasonable agreement with the GATE-mean entrainment zone depth of 183 m reported by Fitzjarrald and Garstang (1981). Just below z_i, a slight increase in stability and drying is evident, a feature also found by Fitzjarrald and Garstang and likely

[2] These mixed layer mean values of q based on the corrected Vaisala H-Humicap data are ~1.5 g kg^{-1} greater than uncorrected values of Loehrer et al. (1996).

related to pronounced dry-air entrainment near z_i (Nicholls and LeMone 1980).

5. Multiscale variability of the mixed layer

a. Time series of mixed layer for IOP

Time series of the mixed layer tops at the four sites are shown in Fig. 7. Also included in the figure is a time series of the IFA-averaged rainfall rate P_0 interpolated to the sounding sites from the data of Curry et al. (1999) and the surface wind speed and buoyancy flux F from IMET. Here, F is defined by $F = S + 0.61c_p\overline{T}E/L$, where E is the latent heat flux, S the sensible heat flux, c_p the specific heat of dry air, L the latent heat of vaporization, and $\overline{T}$ refers to 6-h-averaged surface (10-m) temperature. Shaded bars at the bottom of the top four panels provide an inventory of the sounding data for the four sites.

The surface wind data indicate three westerly wind bursts (WWBs) during the IOP associated with MJO passages: early November, mid-to-late December, and late January. The strongest low-level westerlies were generally preceded 1–3 weeks by heavy rainfall (Lin and Johnson 1996), consistent with the models of Webster (1972) and Gill (1980).[3] A striking result seen in Fig. 7 is the large variability of z_i on multiple timescales. At Kapinga, where the record is nearly continuous, the mixed layer is distinctly modulated by the MJO as convection waxed and waned with this phenomenon. The shallowest mixed layers occurred during periods of heavy precipitation, a pattern particularly noticeable during mid-December and mid-January at Kapinga. Precipitation and z_i were negatively correlated at Kapinga, *Ship 5*, and *Moana Wave* ($r = -0.20$, -0.19, and -0.20, respectively; all significant at the 95% level); however, no significant correlation was found at *Ship 3* ($r = -0.01$). There is no clear explanation for this different behavior at *Ship 3*, but the absence of mixed layers for several days at this site during the rainy period around 20 December may play some role.

The surface buoyancy fluxes at IMET were large during the rainy periods due to increased winds and cooling from precipitation downdrafts. The deepest mixed layers at Kapinga occurred at times of light winds and minimum rainfall in mid-November and late November to early December, and at times of decreasing winds and minimum rainfall around 1 January. Because of data gaps at the ships, the modulation by the MJO is more difficult to detect at these sites. Nevertheless, there does appear to be a reduction in z_i at the time of the heaviest rainfall in mid-December with increasing values of z_i toward the end of the month. However, in early January *Ships 3* and *5* and *Moana Wave* show reduced z_i's whereas Kapinga shows increased values. This difference can be explained by the differing weather conditions across the IFA at this time, with Kapinga lying to the north of disturbed weather that was occurring at the other sites.

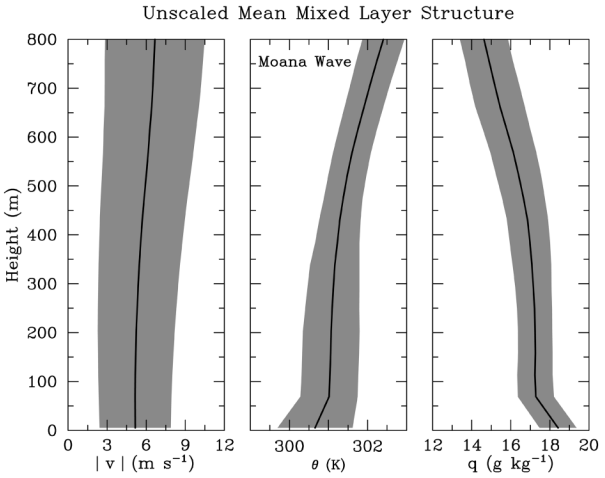

FIG. 6. Unscaled mean mixed layer profile (solid line) and standard deviation (shading) of wind speed (left panel), potential temperature (middle panel) and specific humidity (right panel) for *Moana Wave.*

Another notable feature of the time series of z_i in Fig. 7 is the large variability on short timescales (~6 h to days). Of course, precipitation accounts for much of these short-term fluctuations, but this behavior is even prevalent during nonraining, light-wind periods. Part of this variability is related to the diurnal cycle, a point to be discussed later. However, part must also be due to other factors since the short-period fluctuations occasionally exceed 200–300 m, well above the amplitude of the diurnal cycle. It is not clear what fully accounts for the large short-term variations in z_i during undisturbed conditions, but phenomena that create mesoscale inhomogeneities at those times such as boundary-layer rolls (e.g., Weckwerth et al. 1996) and mesoscale cellular convection (Agee 1984) may play some role. A visible satellite image of the IFA at 1423 LST on 3 December (Fig. 8) is typical of the conditions on undisturbed, light-wind days, showing numerous open, hexagonal cells of ~30-km diameter. During the afternoon on mostly clear, undisturbed days, congestus showers typically formed on the boundaries of such cells in response to the heating of the ocean surface (e.g., Weller and Anderson 1996; Sui et al. 1997a). The ubiquitous nature of such convection is borne out by radar observations by Rickenbach and Rutledge (1997) of precipitation on nearly every day of the three cruises of the R/V *Vickers.* These showers and the mesoscale circulations undoubtedly contributed to the large sounding-to-sounding variability during undisturbed conditions.

[3] Zhang and McPhaden (2000) have shown using buoy data for other years that not all MJOs bear this phase relationship between the wind and rainfall.

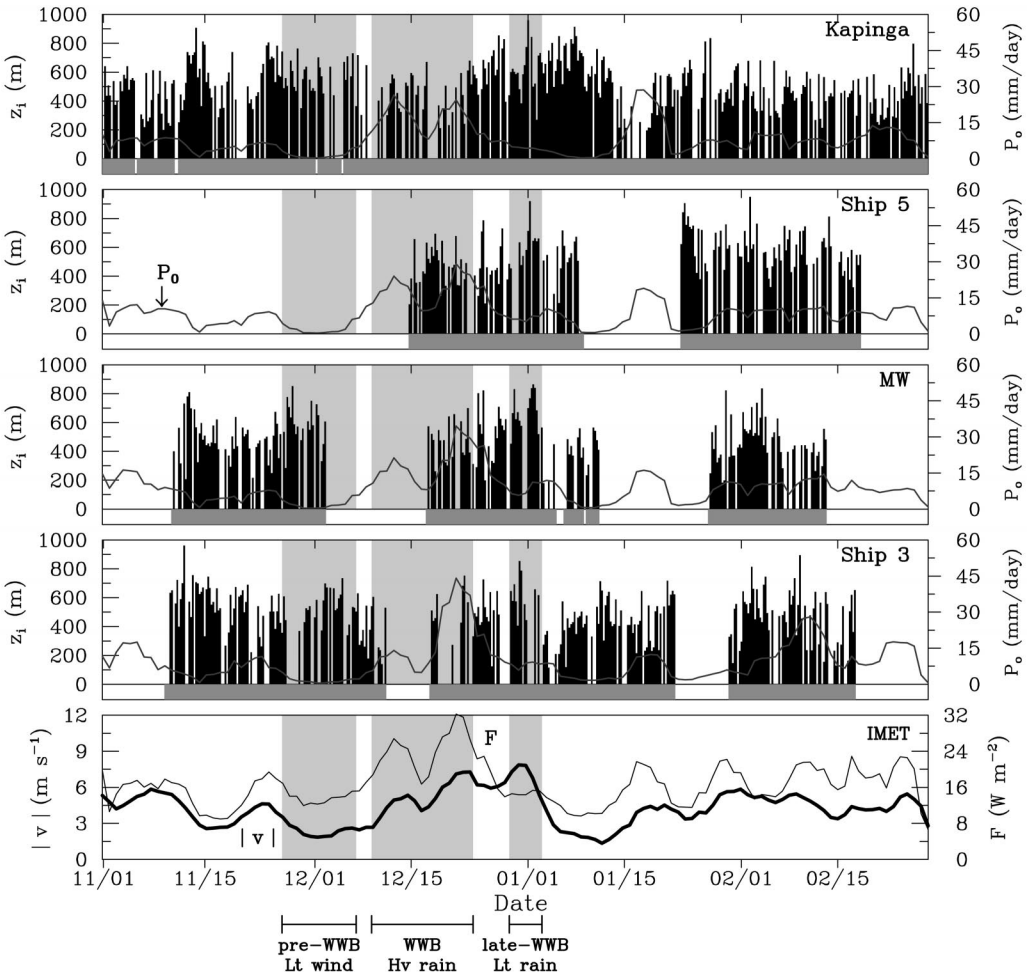

FIG. 7. (top four panels) Time series of mixed layer tops (top of vertical solid bars with scale to left) and 5-day running mean rainfall rate (thin gray line with scale to right) at four sounding sites. Light-shaded regions indicate three periods associated with the passage of an MJO and its associated westerly wind burst (WWB), characterized by different weather conditions noted at the bottom of the figure. Dark-shaded regions at bottom of panels indicate times at which soundings were taken. (bottom panel) Five-day running mean time series of surface wind speed (heavy line with scale to left) and bouyancy flux (thin line with scale to right) at the IMET buoy.

b. *Mixed layer behavior during December westerly wind burst*

To illustrate the variability of the mixed layer on the timescale of the MJO, three periods have been selected centered on the strongest WWB in December: 1) a pre-WWB light-wind period, 27 November–7 December; 2) a WWB heavy-rain period, 10–24 December; and 3) a late-WWB, light-rain period, 30 December–3 January (indicated by shaded regions in Fig. 7). Scaled-mean profiles of wind speed, θ, θ_v, and q averaged for all four sites during these three periods (using only humidity-corrected sondes) are shown in Fig. 9. Mixed layer mean statistics for these three cases are shown in Table 3. In period 1, winds were light (2.4 m s^{-1}) and the mean mixed layer depth $\overline{z}_i$ was 562 m. These values agree well with the aircraft observations of Serra et al. (1997) for their nonconvective class 0 conditions having a mean wind speed of ~2.5 m s^{-1} at 30-m altitude and a $\overline{z}_i$ of ~600 m. During the WWB heavy-rain period 2, much shallower ($\overline{z}_i$ = 466 m) and cooler mixed layers were observed, indicating the frequent occurrence of precipitation downdrafts. Period 3 (late-WWB, light rain) had deep mixed layers ($\overline{z}_i$ = 629 m) and, correspondingly, the warmest and driest conditions. From Fig. 9 it can be seen that, in general, deep mixed layers are warm and dry, whereas shallow mixed layers are cool, though neither anomalously moist nor dry. Histograms of z_i (Fig. 10) show marked shifts in the distributions of mixed layer depths for these three different weather regimes.

To further explore these relationships, scatterplots of z_i and mixed layer mean potential temperature $\overline{\theta}$ and specific humidity $\overline{q}$ are presented in Fig. 11 for all Kapinga mixed layer cases (although Kapinga is not an open-ocean site, it is the only one that has reliable in

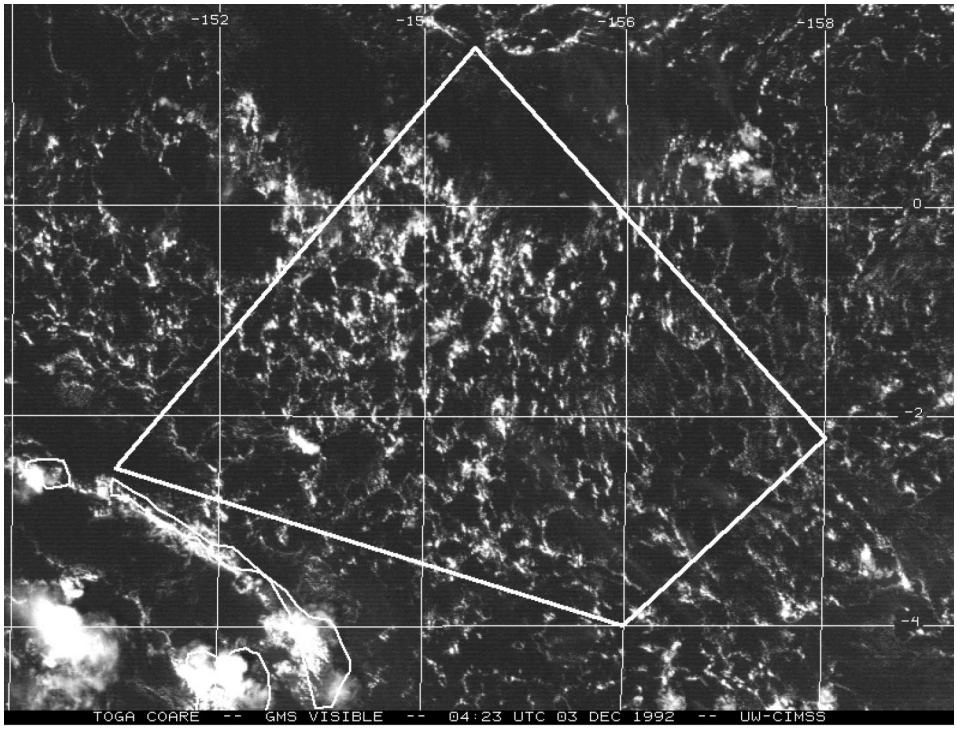

FIG. 8. GMS visible satellite image for 1423 LST on 3 Dec 1992 showing numerous mesoscale open cells of ~30-km diameter within the vicinity of COARE IFA.

situ precipitation data that can be used to relate to mixed layer properties). Soundings with precipitation occurring within 2 h of observation time are indicated with asterisks. It can be seen that z_i is positively correlated with $\overline{\theta}$ ($r = 0.44$) and negatively correlated with $\overline{q}$ ($r = -0.52$), a consequence of deeper mixed layers incorporating higher θ and lower q as they grow. In addition, Fig. 11 shows that the coolest and shallowest mixed layers tend to be associated with recent precipitation events (63% of the soundings with $\overline{\theta} < 300$ K are associated with rain within 2 h of observation time). However, some rain cases also exhibit warm mixed layers. A portion of these were for launches prior to rainfall at the site, but not all. The lack of precise information (e.g., radar) to place the soundings relative to precipitation systems at Kapinga, as well as the coarse 6-h resolution, precludes direct linkage of profiles to rainfall events. There is no clear relationship between $\overline{q}$ and precipitation events, consistent with past observations of both moist and dry air in downdraft wakes (Zipser 1977; Fitzjarrald and Garstang 1981; Johnson and Nicholls 1983; Young et al. 1995).

c. Dry intrusions and the mixed layer

Shown in Fig. 12 is a time series of z_i, the Lifting Condensation Level (LCL), and 600–800-hPa mean q and wind speed at Kapinga. The LCL is computed using mixed layer mean values of θ and q. Its mean value at Kapinga for the IOP is 687 m or 169 m above $\overline{z}_i$ (Table 2). Also listed in Table 2 are average LCLs for the other sites: 723, 741, and 662 m for *Ship 5*, *Moana Wave*, and *Ship 3*, respectively.[4] The lower LCL at *Ship 3* is consistent with the wetter conditions there (Fig. 1). The values of LCL $- z_i$ are in close agreement at three of the sites (Table 2), but it is about 70 m higher at *Moana Wave*. For three of the sites the values of LCL $- z_i$ of ~170 m are physically reasonable since the LCL of the mean mixed layer air (approximately cloud base) is in close proximity to the top of the entrainment zone as it should be (e.g., Malkus 1958), which lies ~100–150 m above z_i (Fig. 5). The value at *Moana Wave* is considerably higher than the others, suggesting a possible slight undercorrection of the humidity at that site. While we cannot confirm this suggestion, it is consistent with $\overline{q}$ at *Moana Wave* being the lowest of all sites (Fig. 5).

The time series of $\overline{q}$ shows periodic drying of the lower troposphere in association with westerly wind bursts. These drying episodes or dry intrusions (e.g., Numaguti et al. 1995), have been found by Yoneyama and Parsons (1999) to lag the maximum westerlies by about 2 days. Numaguti et al. (1995) link the drying events to equatorward flow in westward-propagating

[4] Eighteen, five, and five of the soundings from *Ship 5*, Kapinga, and *Moana Wave*, respectively, were excluded in computing the LCL averages in Table 2 because humidity data were not corrected for these soundings.

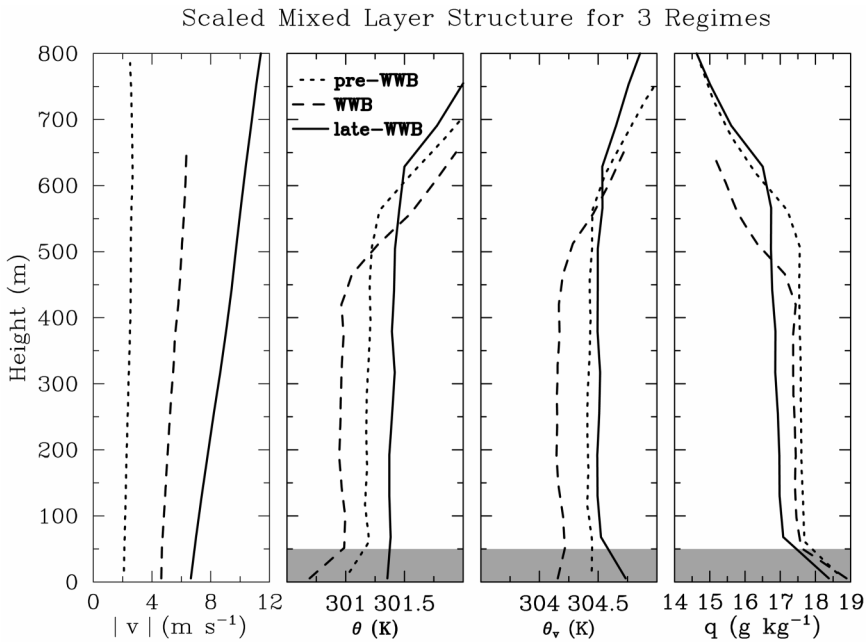

FIG. 9. Scaled mean mixed layer profiles of wind speed (left panel), potential temperature (left-center panel), virtual potential temperature (right-center panel), and specific humidity (right panel) for three WWB regimes computed using data from four sites. Shaded regions in the lowest 50 m of panels indicates questionable thermodynamic data in this layer.

mixed Rossby–gravity waves. They can also be connected with equatorward flow associated with Rossby wave–like disturbances (double cyclone gyres straddling the belt of strong westerlies) accompanying MJO deep convection (Lau et al. 1989; Chen et al. 1996). Yoneyama and Parsons (1999) show through back-trajectory analysis that the dry air can be ultimately traced to the equatorward extension of midlatitude baroclinic waves.

Figure 12 shows that the mixed layer is deepest near times of dry intrusions. The correlation between z_i and $\overline{q}_{600-800}$ is -0.44. This negative correlation may have several possible explanations. First, periods of intense drying tend to suppress convective activity through entrainment effects (Kloesel and Albrecht 1989; Numaguti et al. 1995; Mapes and Zuidema 1996; Brown and Zhang 1997; DeMott and Rutledge 1998) and/or an enhancement of the convective inhibition (Parsons et al. 2000).

TABLE 3. Mixed layer statistics for westerly wind burst. Table includes only those sounding data for which humidity corrections have been applied.

Episode and period (month/day)	No. cases	$\overline{z_i}$ (m)	$\overline{V}$ (m s^{-1})	$\overline{\theta}$ (K)	$\overline{q}$ (g kg^{-1})
1) pre-WWB light wind (11/27–12/07)	73	562	2.4	301.2	17.6
2) WWB heavy rain (12/10–12/24)	96	466	5.3	301.0	17.4
3) late-WWB little rain (12/30–1/03)	56	629	8.8	301.4	16.8

Without deep convection, there are minimal precipitation downdrafts to disrupt the boundary layer and create conditions for shallow mixed layers. Second, dry conditions just above z_i reduce the populations of shallow cumulus clouds (e.g., see Figs. 11 and 12 of shallow cumulus populations from the radar aboard the R/V *Vickers* in Johnson et al. 1999). Since subsidence between cumuli retards the growth of the mixed layer (e.g., Sarachik 1974), a reduction in shallow cumuli should lead to deeper mixed layers. Observations of shallow cumulus populations at Kapinga are not available, but Fig. 12 shows that during the periods of dry intrusions, the LCLs rise to nearly 1 km, consistent with the idea that dry intrusions are inhibiting shallow cumulus development. Finally, Parsons et al. (2000) argue that dry intrusions are associated with a rapid deepening of the mixed layer. Their analysis of the dry intrusion in mid-November showed a sudden jump in the surface latent heat flux to over 200 W m^{-1} over a 12-h period on 13 November at *Moana Wave* as dry air reached the surface. A consequent doubling of the surface buoyancy flux F could indeed have been one of the factors leading to the growth of the mixed layer in mid-November [Eq. (5), later]. However, information on the horizontal extent and duration of such enhanced fluxes is lacking and even contradictory. Specifically, the time series of F at IMET (Fig. 7), in close proximity to *Moana Wave*, shows decreasing values of F from 10 to 15 November.

A further impact of dry intrusions is on the distributions of θ and q in the mixed layer. Referring to Fig.

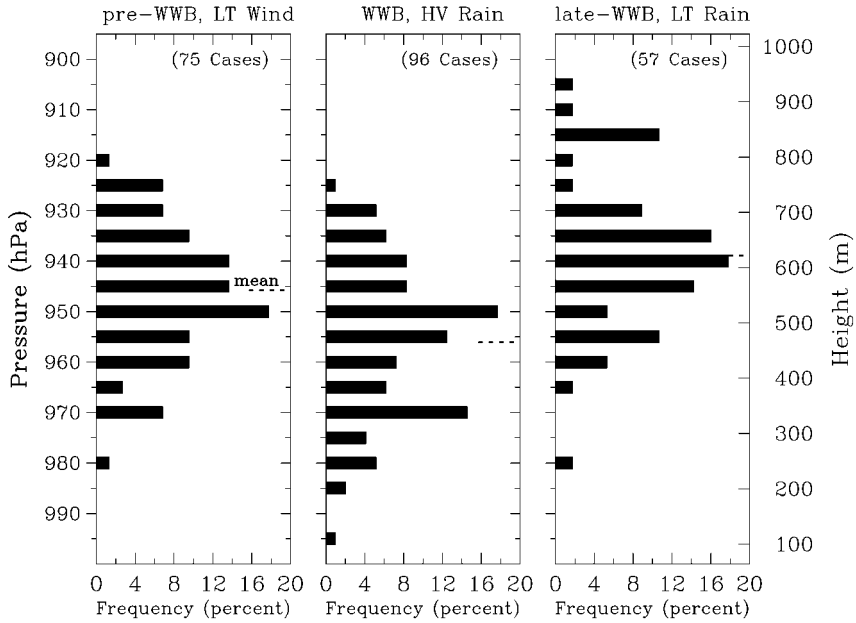

FIG. 10. Histograms for three WWB regimes (computed using data from all four sites) indicating the frequency of occurrence (percent) that a mixed layer top falls within a 5-hPa bin. Number of soundings in each regime that a mixed layer was identified are indicated in parentheses (all sondes considered, not just the humidity-corrected sondes in Table 3). The mean mixed layer top for each regime is indicated with a short dashed line along the right axis of each panel.

9, it can be seen that for the late-WWB, light-rain period (30 December–3 January), which occurred during a time of dry intrusions (Fig. 12), q decreases with height by 0.5 g kg^{-1} throughout the depth of the mixed layer. It is likely that entrainment of very dry air along with mean subsidence is contributing to this profile. A slight increase in θ with height (Fig. 9) also is present for these very deep mixed layers.

6. Analysis of pre-WWB and late-WWB mixed layers

It is clear from Fig. 7 that the mixed layer over the warm pool rarely achieved steady state. However, it is instructive to examine its behavior for several periods during which quasi-steady-state large-scale conditions existed. In particular, the pre-WWB and late-WWB periods were characterized by minimal rainfall and nearly constant surface buoyancy fluxes (Fig. 7), ignoring for the moment diurnal variations.

Assuming radiative heating is the only mixed layer diabatic process, the Reynolds-averaged expression for the virtual potential temperature θ_v is

$$\frac{\partial \overline{\theta}_v}{\partial t} + \overline{\mathbf{v}} \cdot \nabla_H \overline{\theta}_v + \overline{w}\frac{\partial \overline{\theta}_v}{\partial z} = -\frac{\partial \overline{w'\theta_v'}}{\partial z} + Q_R, \quad (1)$$

where Q_R is the radiative heating rate, overbar is a time average (~h), and prime a deviation from that average. Integrating (1) from the top of the surface layer (near $z = 0$) to z_i and assuming well-mixed conditions,

$$\frac{\partial \overline{\theta}_v}{\partial t} + \overline{\mathbf{v}} \cdot \nabla_H \overline{\theta}_v = \frac{F_s - F_i}{\overline{\rho} c_p z_i} + Q_{Rm}, \quad (2)$$

where Q_{Rm} is the mixed layer mean radiative heating rate, F_s and F_i are the buoyancy fluxes (in W m^{-2}) at the surface and z_i, respectively, and ρ is the air density.

For steady-state, horizontally homogeneous conditions,

$$z_i = -\frac{F_s - F_i}{\overline{\rho} c_p Q_{Rm}}, \quad (3)$$

or using the closure $F_i = -kF_s$ for free convection (Ball 1960),

$$z_i = -\frac{(1 + k)F_s}{\overline{\rho} c_p Q_{Rm}}, \quad (4)$$

where k is a positive constant typically between 0.1 and 0.3 (Stull 1976). This expression states that the steady-state mixed layer depth over the ocean is determined by a balance between eddy heat flux convergence and radiative cooling. Betts (1976) notes that the theoretical validity of this simple closure for the case of cumulus-topped mixed layers is not clear; however, if the cloud coverage is small, ~10% or less, then its use is probably tolerable.

Equation (4) can be used to compute a steady-state z_i if Q_{Rm} is known. However, the periods under consideration—the pre-WWB, light-wind period and the late-WWB, light-rain period (Fig. 7)—were not strictly

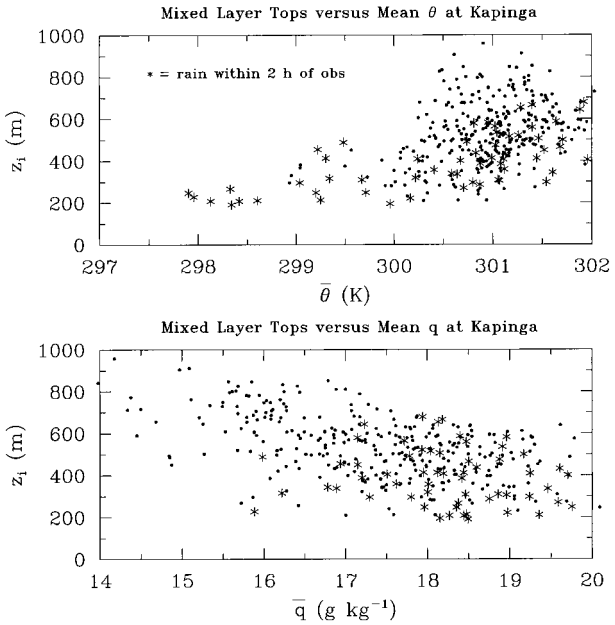

FIG. 11. Scatterplots of mixed layer depth z_i vs mixed layer mean θ (top panel) and mean q (bottom panel) at Kapinga. Asterisks indicate that soundings were launched within two hours of a precipitation event at Kapinga as deduced from tipping bucket gauge data at this site.

steady state, so the full expression (2) must be used.[5] Specifically, the mixed layer warmed during the first period and cooled during the second, while slight cold advection existed during both periods.

Using (2), we compute z_i as a function of Q_{Rm} for the pre- and late-WWB periods. Since surface buoyancy fluxes are not available for all sites, we use IMET values for F_s for the two times: 13.8 and 14.3 W m^{-2} for the pre-WWB and late-WWB periods, respectively. Interestingly, while the late-WWB period exhibits much stronger winds than the pre-WWB period, the values of F_s are not that different (Fig. 7). This observation indicates that factors other than a changing surface buoyancy flux (e.g., a reduction in the shallow cumulus cloud field during dry intrusions, as discussed earlier; a change in the mean vertical motion, etc.) must have accounted for the 12% increase in the mean mixed layer depth in the late-WWB period over that in the pre-WWB period (Table 3). The absence of enhanced buoyancy fluxes during the late-WWB period can be explained by the very small air–sea temperature differences at that time ($\sim$0.1°C), in part due to cooling of the upper ocean by the WWB (Weller and Anderson 1996).

The results for $k = 0.1$, 0.2, 0.3 (the range of published values reported in Stull 1976) for the two periods are shown in Fig. 13. For the pre-WWB period, which is close to the free-convection limit (surface wind speed <2 m s^{-1}), the value of $\overline{z}_i = 562$ m (Table 3) indicates a Q_{Rm} of -1.89 K day^{-1} for $k = 0.2$. In Fig. 13, this value (vertical dashed line) is compared to two independently determined values of Q_{Rm} based on long- and shortwave computations applied to COARE conditions using the NCAR Community Radiation Model (CRM; Kiehl et al. 1994). One is for clear skies and the other for cloudy skies assuming 25% cirrus coverage determined from International Satellite Cloud Climatology Project (ISCCP; Rossow and Schiffer 1991) data with a cirrus layer from 225 to 125 hPa and ice water path of 30 g m^{-2}. The location of the cirrus layer and the estimate of the ice water path are based on lidar and radiometer measurements taken at Kavieng, Papua New Guinea, in January and February 1993 (Platt 1997; Platt et al. 1998). For both the pre- and late-WWB periods, the atmospheric profiles of temperature and moisture required for the CRM computations were obtained using scaled mixed layer data (shown in Fig. 9) below 900 hPa and IFA-averaged data appropriate for the respective time periods above. For the pre-WWB period, the CRM gives $Q_{Rm} = -1.78$ for clear skies and -1.71 K day^{-1} for cloudy skies. These values are at the lower end of the range of estimated Q_{Rm} from the budget (shaded region in Fig. 13).

For the late-WWB period, the CRM estimates of Q_{Rm} are -2.00 and -1.86 for clear and cloudy skies, respectively (assuming 84% cirrus coverage and 40 g m^{-2} ice water path). Sensitivity tests show that very dry conditions just above the mixed layer account for the overall larger cooling rates during the late-WWB period, consistent with the findings of Zhang and Chou (1999) and Parsons et al. (2000). The extensive cirrus coverage during the late-WWB period (e.g., Velden and Young 1994) reduces the cooling rate in the mixed layer from clear-sky values by 7%. The cloudy-sky Q_{Rm} from the CRM agrees quite well with the value of -1.90 K day^{-1} from the mixed-layer budget for $k = 0.2$. The average surface wind speed during the late-WWB period was much stronger, 6.5 m s^{-1}, so wind shear likely also contributed to entrainment at mixed layer top. Using the energy budget expressions in Stull (1976), computations of the surface stress term for the late-WWB period indicate the effective value of k during this period should be doubled over that in the pre-WWB period, which is consistent with the CRM results plotted in Fig. 13.

These findings lead to an important conclusion regarding modulation of mixed-layer depth over the warm pool by cloud and radiative processes. Since the equilibrium mixed layer represents a balance between convergence of heat flux and radiative cooling, processes that alter the radiative cooling can modulate the mixed layer depth. During COARE, as deep convection associated with the MJO moved to the east of the warm pool, extensive cirrus spread westward. This pattern was observed at the end of December (Velden and Young 1994). The cirrus reduced the net tropospheric radiative

[5] Figure 9 indicates slight vertical gradients in θ_v for the two periods, but the vertical advective term in (1) is small enough to be neglected.

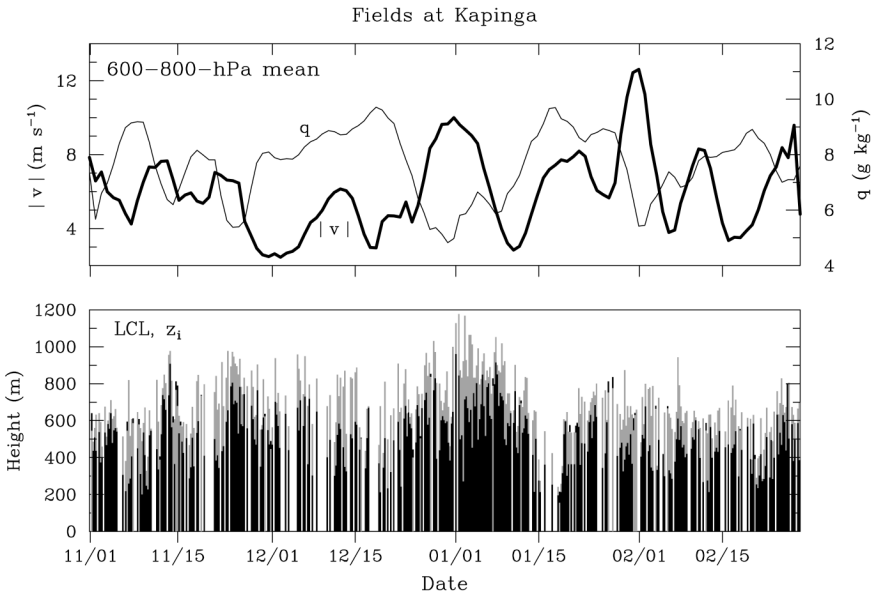

FIG. 12. (top panel) Five-day running mean time series of wind speed (heavy line with scale to left) and specific humidity (thin line with scale to right) averaged in the 600–800-hPa layer at Kapinga. (bottom panel) Time series of LCLs (tops of vertical gray bars) and mixed layer tops (tops of vertical black bars) at Kapinga.

cooling rate (Johnson and Ciesielski 2000) as well as the cooling rate in the boundary layer over its clear-sky value by 7%. On the other hand, mixed layer drying just above the mixed layer at the end of the WWB period enhanced clear-sky cooling in the mixed layer over its pre-WWB value by 11%. This drying was also associated with the MJO, in this instance through equatorward advection of dry air in Rossby wave–like disturbances or double-cyclone gyres to the west of the deep convection (Lau et al. 1989; Chen et al. 1996). The net effect of these processes was a slightly enhanced mixed layer radiative cooling rate during the late-WWB period. Computations from (2) show that all three processes—storage, advection, and radiation—were important factors in regulating the mixed layer depth during both the pre- and late-WWB periods.

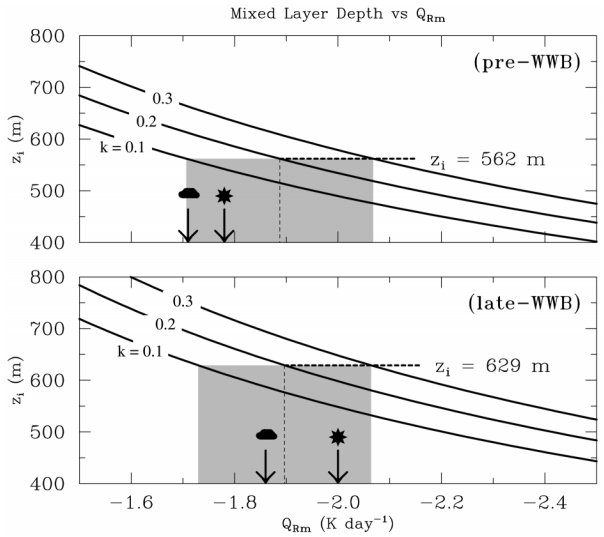

FIG. 13. Solution of the θ_v mixed layer equation [see (2) in the text] for $k = 0.1$, 0.2, 0.3 (solid curves) for the pre-WWB period (top panel) and late-WWB period (bottom panel). For the mean z_i associated with each period, the vertical dashed line indicates the diagnosed value of Q_{Rm} for $k = 0.2$ while the shaded region shows the range of diagnosed Q_{Rm} values for $0.1 \leq k \leq 0.3$. The arrows with the cloud (sun) symbols over them represent independent Q_{Rm} estimates determined using a radiation model with (without) cirrus clouds. See text for details.

7. The diurnal cycle

It is normally argued that diurnal variations of the atmospheric boundary layer over the ocean are negligible owing to the very small diurnal cycle of the SST. This statement is true over many regions of the globe. However, the warm pool is unique in that prolonged clear-sky, light-wind conditions lead to a relatively large diurnal cycle of the SST (up to 2°–3°C) and surface fluxes (Weller and Anderson 1996). Correspondingly, observations show a diurnally varying mixed layer depth in response to those fluxes.

To remove effects of rainfall and isolate the diurnal cycle, soundings for the pre-WWB, light-wind period are examined. Scaled-mean profiles of wind speed, θ, θ_v, and q for this period are shown for *Ship 3* in Fig. 14. As in Fig. 5, near-surface values of θ and q are not considered reliable. The sample size is limited (26 total soundings not equally distributed by time of day); nevertheless, a clear diurnal cycle of boundary-layer evo-

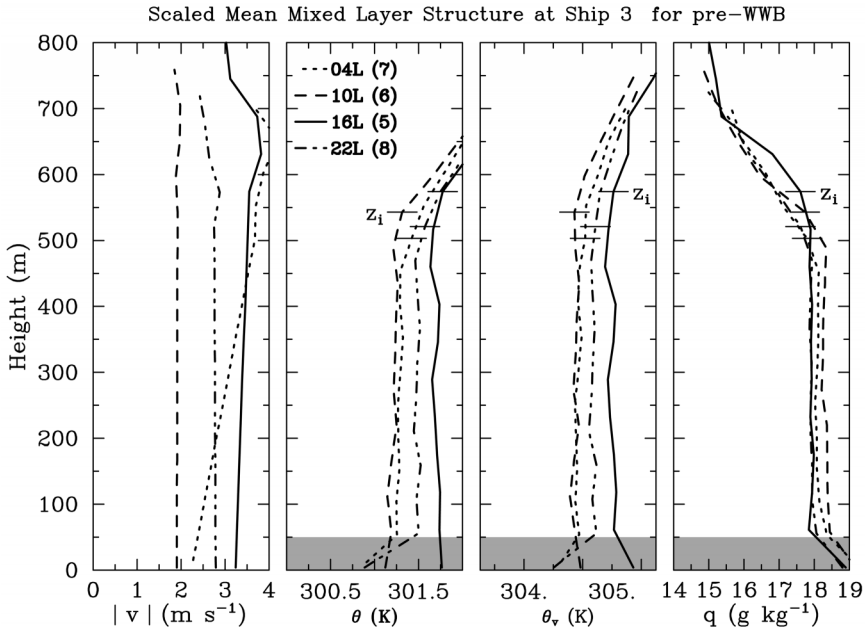

FIG. 14. Scaled mean mixed layer profiles at 0400, 1000, 1600, and 2200 LST of wind speed (left panel), potential temperature (left-center panel), virtual potential temperature, (right-center panel), and specific humidity (right panel) at *Ship 3* for the pre-WWB period. Mean values of the mixed layer top are indicated with short solid lines intersecting the θ, θ_v, and q curves. Shaded regions in the lowest 50 m of the panels indicate questionable thermodynamic data in this layer. Number of cases are indicated in parentheses.

lution can be seen reminiscent of that over land. The deepest and warmest mixed layers are in the afternoon (574 m at 1600 LST) and the shallowest are at night (502 m at 0400 LST), a 14% variation about the mean. Although this diurnal variation of z_i falls shy of being significant at the 0.05 level using a chi-square test, the results are physically reasonable in terms of a diurnal heating of the boundary layer by the SST. Specifically, the diurnal cycle of SST on light-wind days (1.1 K amplitude at IMET for the pre-WWB period) is sufficiently large to drive a noticeable diurnal cycle in the boundary layer structure including an afternoon mixed layer warming of 0.5 K.[6] Slightly stable conditions are seen in the morning (through most of the mixed layer above 100 m), while near-neutral to slightly unstable conditions are observed in the afternoon and early night. Strongest wind speeds at low levels occur at 1600 LST, with weakest winds at 1000 LST. The phase of the wind speed cycle in Fig. 14 is consistent with semidiurnal and diurnal harmonics of wind profiler data for *Ship 3* reported by Gutzler and Hartten (1995) and of surface buoy wind data for the western Pacific (Deser and Smith 1998). The mixed layer evolution for the daytime is similar to that reported by Serra et al. (1997) based on aircraft missions in the COARE undisturbed boundary layer.

The diurnal cycle at Kapinga during the pre-WWB period is even more pronounced with a rise from 460 to 625 m, or 30% variation about the mean (Fig. 15). Moreover, the mixed layer there exhibits a 0.7 K warming and 0.7 g kg^{-1} drying from night to day. The wind speeds at Kapinga were very light during this period (1–2 m s^{-1}), increasing slightly in the afternoon. The large amplitude of the diurnal cycle at Kapinga is probably not represenative of the open ocean since it may be influenced by heating of the land areas and/or lagoons on this small atoll during very light winds.

To interpret the diurnal cycle of the mixed layer under clear-sky, light-wind conditions, Fig. 16 has been prepared showing the diurnal variation of wind speed, SST, air temperature, and surface buoyancy flux from the IMET; z_i and LCL (based on mixed layer mean θ and q) for *Ship 3*; and fractional cloudiness from the *Moana Wave* ceilometer[7] for the pre-WWB period. *Ship 3* is used to depict the diurnal cycle because it is representative of open-ocean conditions and its time on station for the pre-WWB period was the longest of the ships (Table 1 or Fig. 7). SST, wind speed, and the buoyancy flux F_s at IMET peak shortly after noon, with a large (14 W m^{-2}) variation in F_s (Figs. 16a,b). The diurnal variation of F_s closely matches that of the SST minus air temperature difference and to a lesser extent that of

[6] Parsons et al. (2000) note that absorption of solar short wave radiation, primarily by water vapor, also contributes to the afternoon mixed layer warming.

[7] The ceilometer data extend only through 3 December, when the first cruise of *Moana Wave* ended (Table 1).

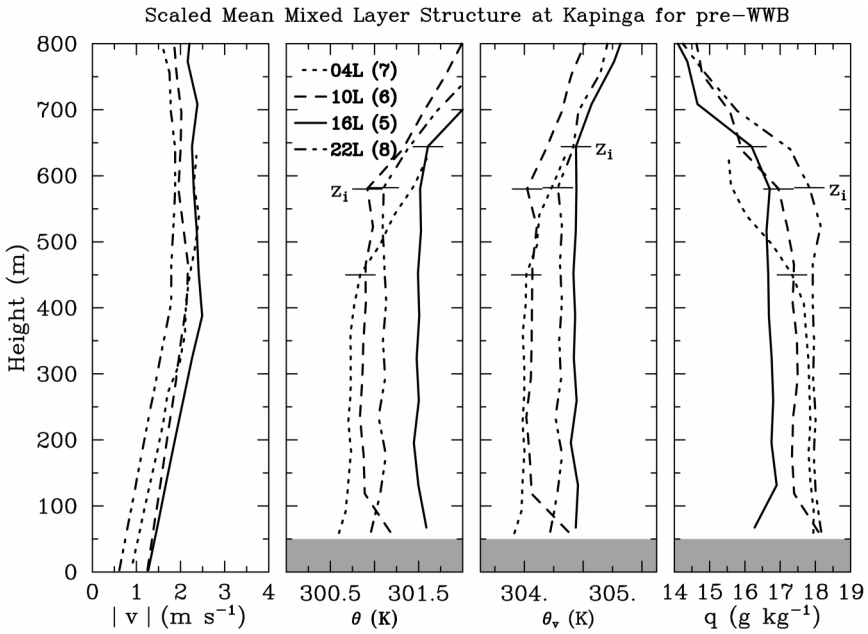

FIG. 15. Scaled mean mixed layer profiles at 0400, 1000, 1600, and 2200 LST of wind speed (left panel), potential temperature (left-center panel), virtual potential temperature (right-center panel), and specific humidity (right panel) at Kapinga for the pre-WWB period. Mean values of the mixed layer top are indicated with short solid lines intersecting the θ and q curves. Thermodynamic data below 50 m are unreliable. Number of cases are indicated in parentheses.

the wind speed. The prediction equation for z_i (assuming the fractional area occupied by shallow cumulus is $\ll 1$) from the zero-order jump model (Lilly 1968; Tennekes 1973) is

$$\frac{\partial z_i}{\partial t} = \overline{w}_i + \frac{kF_s}{\rho c_p \Delta}, \tag{5}$$

where $\overline{w}_i$ is the vertical velocity at z_i and Δ is the inversion strength atop the mixed layer. A predictive equation for Δ can also be derived (Tennekes 1973) that along with (5) forms a coupled set that can be solved for z_i, Δ assuming $\overline{w}_i$ is known. Unfortunately, $\overline{w}_i$ is difficult to determine accurately enough from the sounding network to permit a solution of the coupled system. However, assuming $\overline{w}_i$ and Δ do not change markedly over the diurnal cycle (Tennekes 1973 shows that for $\overline{w}_i = 0$, $\Delta \propto z_i$), the evolution of z_i over the course of a day (Fig. 16c) is qualitatively consistent with the evolution of F_s based on (5). More quantitative comparisons are precluded by the coarse (6-h) resolution of the sounding data, the lack of colocated surface fluxes, and the inability to accurately determine $\overline{w}_i$.

The *Moana Wave* ceilometer data (Fig. 16d) show a prominent afternoon maximum in fractional cloudiness, which corresponds closely to the diurnal variation of z_i. Since the ceilometer does not detect clouds above 3.5 km (White et al. 1995), and radar data indicate cumulonimbus were not present during this period (Fig. 9 of Johnson et al. 1999), these clouds are predominantly shallow cumulus and cumulus congestus. The development of these clouds can be explained by considering the diurnal variation of z_i and LCL (Fig. 16c). Following a decrease from 2200 to 0400 LST, the LCL is nearly constant during the early morning hours. The reduction in the LCL during the night is due to mixed layer cooling and moistening (Fig. 15 and Sui et al. 1997a). The moistening at night can be attributed to a reduction in shallow cumulus, which serve to transport moisture out of the mixed layer (Esbensen 1978). As the mixed layer grows in the morning, the difference between z_i and LCL decreases to less than 125 m, thereby promoting the development of shallow cumulus by overshooting boundary-layer plumes or thermals. As z_i continues to grow into the afternoon, clouds continue to increase. However, in the late afternoon, the LCL increases to nearly 200 m above z_i due to mixed layer drying by cumulus transport and the downward entrainment of dry air, leading to a decrease in the shallow cumulus population. The large diurnal variation in the surface buoyancy flux of 14 W m^{-2} (Fig. 16) clearly plays a role in the growth of the mixed layer and afternoon cumulus development, although absorption of solar shortwave radiation in the boundary layer can also contribute by removing convective inhibition (Parsons et al. 2000).

Thus, on clear, light-wind days, the boundary layer over the warm pool behaves like land: SST increases in the afternoon, the bouyancy flux increases, and the mixed layer grows. Of course, the amplitude is less than that over land, but the implications are important. The growth in the boundary layer contributes to the devel-

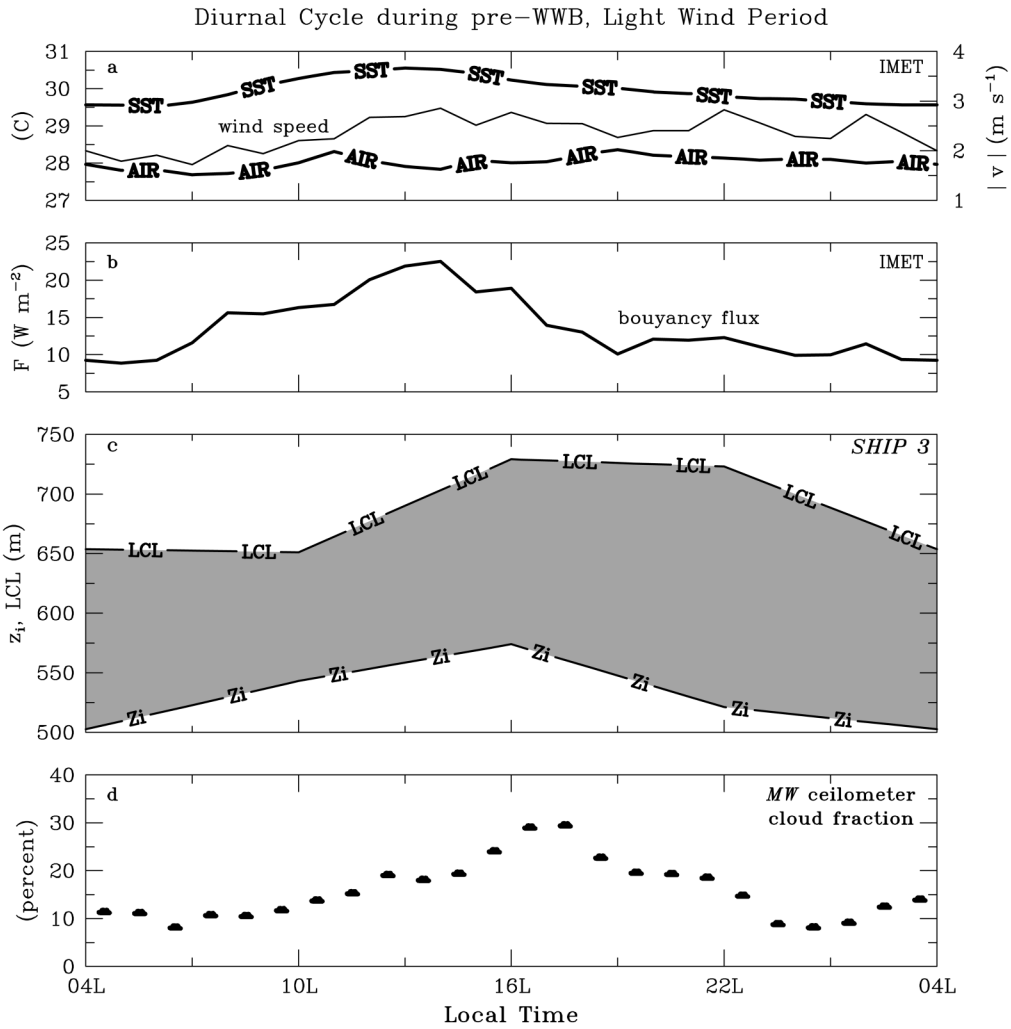

FIG. 16. Diurnal cycle during the pre-WWB, light-wind period of (a) SST and air temperature at IMET (labeled curves with scale on left) and surface wind speed at IMET (thin curve with scale to right), (b) surface bouyancy flux at IMET, (c) z_i and LCL at *Ship 3*, and (d) cloud fraction determined by the ceilometer aboard the *Moana Wave*.

opment of afternoon showers (Chen and Houze 1997; Rickenbach and Rutledge 1997; Sui et al. 1997a) and organized mesoscale circulations (Fig. 8). Most of the showers at these times are from congestus clouds topping out in the midtroposphere (Zuidema 1998; Johnson et al. 1999). While these clouds rain, they do so inefficiently, thereby moistening the low- to midtroposphere (Raymond and Torres 1998). Without the diurnal cycle, precipitation over the warm pool and its associated moistening would likely be far less during the suppressed phase of the MJO. Thus, the additional impetus provided by the diurnal cycle in enhancing congestus cloud growth during the MJO suppressed phase may be an essential aspect of preconditioning the environment for deep convection in the MJO active phase (Johnson et al. 1999). This preconditioning likely plays a key role in setting the timescale for the MJO (Bladé and Hartmann 1993; Hu and Randall 1994; Kemball-Cook and Weare 2001). Webster et al. (1996) already discussed the importance of this nonlinearity in the context of numerical simulations, pointing out that proper representation of the diurnal cycle of SST is essential to modeling the correct feedback between clouds and SST, and preventing errors in the simulation of the large-scale circulation.

Finally, we use (2), neglecting the effects of horizontal advection on the diurnal timescale, to determine the diurnal cycle of radiative cooling in the mixed layer. We consider the undisturbed, pre-WWB period for this computation using data only from Kapinga and *Ship 3* since observations from the other sites are limited. The average Q_{Rm} based on the solution of (2) for Kapinga and *Ship 3* (using F_s from IMET) is shown in Fig. 17. The points refer to values computed using $k = 0.2$, with

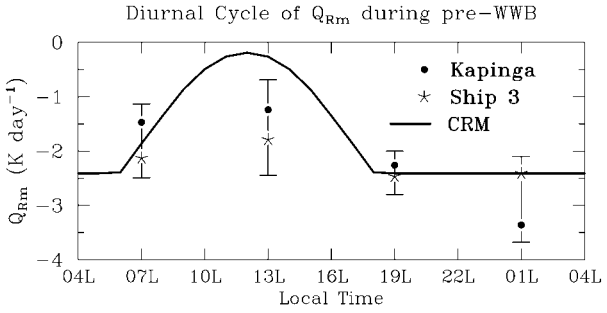

FIG. 17. Diagnosed values of Q_{Rm} using the θ_v mixed layer equation [neglecting the effects of horizontal advection in (2)] with $k = 0.2$ using data for the pre-WWB period data from Kapinga (filled circles) and *Ship 3* (asterisks). Overlapping error bars are shown for the two sites. Solid line shows a radiative model (CRM) estimate using a pre-WWB sounding assuming 25% cirrus coverage.

error bars indicating the range of results for k between 0.1 and 0.3 and for errors in F_s of 10%. The observations show a Q_{Rm} ranging from about -1.5 K day^{-1} during midday to nearly -3 K day^{-1} at night (a daily mean of -2.1 K day^{-1}). Also plotted in Fig. 17 are results using the NCAR CRM with the mean pre-WWB sounding and a 25% cirrus coverage (as deduced from ISCCP data). The diagnosed and CRM results are in reasonably good agreement considering the range of possible errors in both observations and modeling, and point to the significant amplitude of midday shortwave radiative heating (Parsons et al. 2000).

8. Summary and conclusions

Six-hourly soundings (1283 total) from Kapingamarangi and R/V's *Moana Wave*, *Shiyan 3*, and *Xiangyanghong 5* have been used to determine the properties of the atmospheric mixed layer over the western Pacific warm pool during TOGA COARE. The main findings of this paper are listed below. Importantly, the first two are consistent with results from the GARP Atlantic Tropical Experiment, while the remaining findings represent new results for the warm pool region.

- Nearly three-quarters (926) of the soundings had identifiable mixed layers. Most of the remainder exhibited stable stratification in the boundary layer as a result of cooling by rainfall evaporation. It is estimated that approximately 40%–50% of the total soundings in COARE were influenced by precipitation downdrafts.
- The mean mixed layer depth was 512 m with large variations on multiple timescales (standard deviation = 155 m, range from 116 to 961 m).
- A west-to-east decrease in the mean mixed layer depth was observed across the warm pool—from 553 m at *Ship 5* in the west to 491 m at *Ship 3* in the east, consistent with the west-to-east increase in mean rainfall rates.
- Significant modulation of the mixed layer occurred on the timescale of the Madden–Julian oscillation (MJO). The mean mixed layer depth
  - — was 562 m during the undisturbed, light-wind period prior to the strong westerly wind burst (WWB) associated with the December MJO;
  - — decreased to 466 m during the heavy-rain period of the WWB, reflecting numerous, recovering precipitation downdraft wakes;
  - — increased to 629 m during the late stages of the WWB when precipitation ended.
- Dry intrusions over the warm pool caused the mixed layer to deepen, at times to 800 m and more. Since the surface buoyancy flux typically did not increase at these times, the deepening is linked to a suppression of shallow cumulus clouds by the dry air (reduced between-cloud subsidence) as well as a general reduction in the overall shower activity and associated precipitation downdrafts.
- Storage, advective, and radiative effects all played important roles in the thermodynamic budget for the mixed layer during the pre- and late-WWB periods. Radiative model results indicate that mixed layer net radiative cooling increased from ~ -1.7 to -1.9 K day^{-1} from the pre-WWB to the late-WWB period, primarily as a result of strong drying just above the mixed layer. The enhanced mixed layer radiative cooling occurred despite extensive cirrus coverage at the end of the December westerly wind burst, which acted in the opposite direction, namely, to reduce the radiative cooling rate over its clear-sky value.
- A diurnal cycle in the mixed layer depth is observed, with maximum amplitude in undisturbed, light-wind conditions. The mixed layer is deepest and warmest in the afternoon in direct response to 1) an afternoon peak in the surface buoyancy flux which, in turn, arose from a large diurnal cycle in SST (up to 2°–3°C) on light-wind days, and 2) absorption of solar shortwave radiation (Parsons et al. 2000). Thus, the atmospheric mixed layer over the warm pool during undisturbed conditions behaves like that over land, albeit with a weaker diurnal cycle amplitude, but sufficient enough to generate an afternoon maximum in shallow cumulus clouds. The additional impetus provided by the diurnal cycle in enhancing congestus cloud growth during the MJO suppressed phase may be an essential aspect of preconditioning the environment for deep convection in the MJO active phase.
- Diagnosis of the mixed layer net radiative cooling rate during pre-WWB, light-wind conditions indicates a large diurnal range, from ~ -1.5 K day^{-1} at midday to nearly -3 K day^{-1} at night.

These findings are based on the recently released humidity-corrected COARE sounding data. Mixed layer mean values of specific humidity in the corrected dataset, ranging from 17.2 to 17.9 g kg^{-1}, are in good agreement with independently determined ~17–18 g kg^{-1} values from aircraft flights in undisturbed condi-

tions (Serra et al. 1997; LeMone et al. 1998). Comparisons of the lifting condensation levels (LCLs) at the four sites with the top of the entrainment zone are consistent except at *Moana Wave*, suggesting a possible slight undercorrection to the relative humidity at that site. However, further intercomparisons are recommended before definitive conclusions are drawn.

Broadly, the results of this study indicate large variablity of the atmospheric mixed layer over the warm pool on multiple timescales, including that of the MJO. In fact, the significant deepening of the mixed layer during the latter stage of the strong December westerly wind burst suggests yet additional modulating factors for the MJO itself. In particular, the extremely dry conditions in the lower troposphere following the passage of deep convection (Fig. 12) inhibit deep convection and associated downdrafts, thereby allowing the mixed layer to grow. Once the mixed layer has grown sufficiently (to 800 m or more), shallow cumulus will again be favored, leading to a subsequent moistening of the lower troposphere. Thus, the growth of the mixed layer provides a mechanism for the remoistening of the lower troposphere following dry intrusions associated with the MJO.

Acknowledgments. This research has been supported by the National Oceanic and Atmospheric Administration, under Grants NA37RJ0202 and NA67RJ0152, and by the National Aeronautics and Space Administration under Grant NAG5-9665. We thank Jason Knievel for his assistance in preparing some figures, Richard Austin and Martin Platt for their help in determining the values of the cloud parameters to use in the radiative transfer calculation, Allen While for the *Moana Wave* ceilometer data, and Chris Velden for satellite imagery. We also acknowledge helpful discussions with Tom Rickenbach and Yolande Serra, and valuable suggestions from three anonymous reviewers.

REFERENCES

Agee, E. M., 1984: Observations from space and thermal convection: A historical perspective. *Bull. Amer. Meteor. Soc.,* **65,** 938–949.

Anderson, S. P., R. A. Weller, and R. B. Lukas, 1996: Surface buoyancy forcing and the mixed layer of the Western Pacific warm pool: Observations and one-dimensional model results. *J. Climate,* **9,** 3056–3085.

Augstein, E., H. Schmidt, and F. Ostapoff, 1974: The vertical structure of the atmospheric boundary layer in undisturbed trade winds over the Atlantic. *Bound.-Layer Meteor.,* **6,** 129–150.

Ball, F. K., 1960: Control of inversion height by surface heating. *Quart. J. Roy. Meteor. Soc.,* **86,** 483–494.

Betts, A. K., 1976: Modeling subcloud layer structure and interaction with a shallow cumulus layer. *J. Atmos. Sci.,* **33,** 2363–2382.

Bladé, I., and D. L. Hartmann, 1993: Tropical intraseasonal oscillations in a simple nonlinear model. *J. Atmos. Sci.,* **50,** 2922–2939.

Bond, N. A., 1992: Observations of planetary boundary layer structure in the eastern equatorial Pacific. *J. Climate,* **5,** 699–706.

Brown, R. G., and C. Zhang, 1997: Variability of midtropospheric moisture and its effect on cloud-top height distribution during TOGA COARE. *J. Atmos. Sci.,* **54,** 2760–2774.

Brümmer, B., 1978: Mass and energy budgets of a 1-km high atmospheric box over the GATE C-scale triangle during undisturbed and disturbed weather conditions. *J. Atmos. Sci.,* **35,** 997–1011.

Bunker, A. F., B. Haurwitz, J. S. Malkus, and H. Stommel, 1949: Vertical distribution of temperature and humidity over the Caribbean Sea. *Pap. Phys. Oceanogr. Meteor.,* **11,** 1–82.

Chen, S. S., and R. A. Houze Jr., 1997: Diurnal variation and lifecycle of deep convective systems over the tropical Pacific warm pool. *Quart. J. Roy. Meteor. Soc.,* **123,** 357–388.

——, ——, and B. E. Mapes, 1996: Multiscale variability of deep convection in relation to large-scale circulation in TOGA COARE. *J. Atmos. Sci.,* **53,** 1380–1409.

Ciesielski, P. E., L. M. Hartten, and R. H. Johnson, 1997: Impacts of merging profiler and rawinsonde winds on TOGA COARE analyses. *J. Atmos. Oceanic Technol.,* **14,** 1264–1279.

Curry, J. A., C. A. Clayson, W. B. Rossow, R. Reeder, Y.-C. Zhang, P. J. Webster, G. Liu, and R.-S. Sheu, 1999: High-resolution satellite-derived dataset of the surface fluxes of heat, freshwater, and momentum for the TOGA COARE IOP. *Bull. Amer. Meteor. Soc.,* **80,** 2059–2080.

DeMott, C. A., and S. A. Rutledge, 1998: The vertical structure of TOGA COARE convection. Part II: Modulating influences and implications for diabatic heating. *J. Atmos. Sci.,* **55,** 2748–2762.

Deser, C., and C. A. Smith, 1998: Diurnal and semidiurnal variations of the surface wind field over the tropical Pacific Ocean. *J. Climate,* **11,** 1730–1748.

Esbensen, S. K., 1978: Bulk thermodynamic effects and properties of small tropical cumuli. *J. Atmos. Sci.,* **35,** 826–837.

——, and M. J. McPhaden, 1996: Enhancement of tropical ocean evaporation and sensible heat flux by atmospheric mesoscale systems. *J. Climate,* **9,** 2307–2325.

Firestone, J. K., and B. A. Albrecht, 1986: The structure of the atmospheric boundary layer in the central equatorial Pacific during January and February of FGGE. *Mon. Wea. Rev.,* **114,** 2219–2231.

Fitzjarrald, D. R., and M. Garstang, 1981: Boundary-layer growth over the tropical ocean. *Mon. Wea. Rev.,* **109,** 1762–1772.

Flament, P., J. Firing, M. Sawyer, and C. Trefois, 1994: Amplitude and horizontal structure of a large diurnal sea surface warming event during the Coastal Ocean Dynamics Experiment. *J. Phys. Oceanogr.,* **24,** 124–139.

Flatau, M., P. Flatau, P. Phoebus, and P. P. Niiler, 1997: The feedback between equatorial convection and local radiative and evaporative processes: The implications for intraseasonal oscillations. *J. Atmos. Sci.,* **54,** 2373–2386.

Gaynor, J. E., and C. F. Ropelewski, 1979: Analysis of the convectively modified GATE boundary layer using *in situ* and acoustic sounder data. *Mon. Wea. Rev.,* **107,** 985–993.

Geldmeier, M. F., and G. M. Barnes, 1997: The ''footprint'' under a decaying tropical mesoscale convective system. *Mon. Wea. Rev.,* **125,** 2879–2895.

Gill, A. E., 1980: Some simple solutions for heat-induced tropical circulation. *Quart. J. Roy. Meteor. Soc.,* **106,** 447–462.

Godfrey, J. S., R. A. Houze Jr., R. H. Johnson, R. Lukas, J.-L. Redelsperger, A. Sumi, and R. Weller, 1998: Coupled Ocean–Atmosphere Response Experiment (COARE): An interim report. *J. Geophys. Res.,* **103,** 14 395–14 450.

Guichard, F., D. Parsons, and E. Miller, 2000: Thermodynamical and radiative impact of the correction of sounding humidity bias in the Tropics. *J. Climate,* **13,** 3611–3624.

Gutzler, D. S., and L. M. Hartten, 1995: Daily variability of lower tropospheric winds over the tropical western Pacific. *J. Geophys. Res.,* **100,** 22 999–23 008.

Halpern, D., and R. K. Reed, 1976: Heat budget of the upper ocean under light winds. *J. Phys. Oceanogr.,* **6,** 972–975.

Hendon, H. H., and J. Glick, 1997: Intraseasonal air–sea interaction

in the tropical Indian and Pacific Oceans. *J. Climate,* **10,** 647–661.
Houze, R. A., Jr., 1977: Structure and dynamics of a tropical squall-line system observed during GATE. *Mon. Wea. Rev.,* **105,** 1540–1567.
Hu, Q., and D. A. Randall, 1994: Low-frequency oscillations in radiative–convective systems. *J. Atmos. Sci.,* **51,** 1089–1099.
Jabouille, P., J. L. Redelsperger, and J. P. Lafore, 1996: Modification of surface fluxes by atmospheric convection in the TOGA COARE region. *Mon. Wea. Rev.,* **124,** 816–837.
Johnson, R. H., and M. E. Nicholls, 1983: A composite analysis of the boundary layer accompanying a tropical squall line. *Mon. Wea. Rev.,* **111,** 308–319.
——, and X. Lin, 1997: Episodic trade-wind regimes over the western Pacific warm pool. *J. Atmos. Sci.,* **54,** 2020–2034.
——, and P. E. Ciesielski, 2000: Rainfall and radiative heating rates from TOGA COARE atmospheric budgets. *J. Atmos. Sci.,* **57,** 1497–1514.
——, T. M. Rickenbach, S. A. Rutledge, P. E. Ciesielski, and W. H. Schubert, 1999: Trimodal characteristics of tropical convection. *J. Climate,* **12,** 2397–2433.
Jorgensen, D. P., M. A. LeMone, and S. B. Trier, 1997: Structure and evolution of the 22 February 1993 TOGA COARE squall line: Aircraft observations of precipitation, circulation, and surface energy fluxes. *J. Atmos. Sci.,* **54,** 1961–1985.
Kemball-Cook, S. R., and B. C. Weare, 2001: The onset of convection in the Madden-Jullian oscillation. *J. Climate,* **14,** 780–793.
Kiehl, J. T., J. J. Hack, and B. P. Briegleb, 1994: The simulated Earth radiation budget of the National Center for Atmospheric Research community climate model CCM2 and comparisons with the Earth Radiation Budget Experiment (ERBE). *J. Geophys. Res.,* **99,** 20 815–20 827.
Kingsmill, D. E., and R. A. Houze Jr., 1999: Thermodynamic characteristics of air flowing into and out of precipitating convection over the west Pacific warm pool. *Quart. J. Roy. Meteor. Soc.,* **125,** 1209–1229.
Kloesel, K. A., and B. A. Albrecht, 1989: Low-level inversions over the tropical Pacific—Thermodynamic structure of the boundary layer and above-inversion moisture structure. *Mon. Wea. Rev.,* **117,** 87–101.
Lau, K.-M., L. Peng, C.-H. Sui, and T. Nakazawa, 1989: Dynamics of super cloud clusters, westerly wind burst, 30–60 day oscillation, and ENSO: A unified view. *J. Meteor. Soc. Japan,* **67,** 205–219.
LeMone, M. A., and W. T. Pennell, 1976: The relationship of trade wind cumulus distribution to subcloud layer fluxes. *Mon. Wea. Rev.,* **104,** 524–539.
——, E. J. Zipser, and S. B. Trier, 1998: The role of environmental shear and thermodynamic conditions in determining the structure and evolution of mesoscale convective systems during TOGA COARE. *J. Atmos. Sci.,* **55,** 3493–3518.
Lilly, D. K., 1968: Models of cloud-topped mixed layers under a strong inversion. *Quart J. Roy. Meteor. Soc.,* **94,** 292–309.
Lin, X., and R. H. Johnson, 1996: Kinematic and thermodynamic characteristics of the flow over the western Pacific warm pool during TOGA COARE. *J. Atmos. Sci.,* **53,** 695–715.
Loehrer, S. M., T. A. Edmands, and J. A. Moore, 1996: TOGA COARE upper-air sounding data archive: Development and quality control procedures. *Bull. Amer. Meteor. Soc.,* **77,** 2651–2671.
Lucas, C., and E. J. Zipser, 2000: Environmental variability during TOGA COARE. *J. Atmos. Sci.,* **57,** 2333–2350.
Lukas, R., 1991: The diurnal cycle of sea surface temperature in the western equatorial Pacific. *TOGA Notes,* **2,** 1–5.
——, and E. Lindstrom, 1991: The mixed layer of the western equatorial Pacific Ocean. *J. Geophys. Res.,* **96,** 3343–3357.
Madden, R. A., and P. R. Julian, 1971: Detection of a 40–50 day oscillation in the zonal wind in the tropical Pacific. *J. Atmos. Sci.,* **28,** 702–708.
Malkus, J. S., 1958: On the structure of the trade-wind moist layer. *Pap. Phys. Oceanogr. Meteor.,* **13,** 1–47.
Mapes, B. E., and P. Zuidema, 1996: Radiative-dynamical consequences of dry tongues in the tropical atmosphere. *J. Atmos. Sci.,* **53,** 620–638.
Nicholls, S., and M. A. LeMone, 1980: The fair weather boundary layer in GATE: The relationship of subcloud fluxes and structure to the distribution and enhancement of cumulus clouds. *J. Atmos. Sci.,* **37,** 2051–2067.
Numaguti, A., R. Oki, K. Nakamura, K. Tsuboki, N. Misawa, T. Asai, and Y.-M. Kodama, 1995: 4–5-day-period variations and low-level dry air observed in the equatorial western Pacific during the TOGA-COARE IOP. *J. Meteor. Soc. Japan,* **73,** 267–290.
Parsons, D., and Coauthors, 1994: The Integrated Sounding System: Description and preliminary observations from TOGA COARE. *Bull. Amer. Meteor. Soc.,* **75,** 553–567.
——, K. Yoneyama, and J.-L. Redelsperger, 2000: The evolution of the tropical western Pacific atmosphere–ocean system following the arrival of a dry intrusion. *Quart. J. Roy. Meteor. Soc.,* **126,** 517–548.
Pennell, W. T., and M. A. LeMone, 1974: An experimental study of turbulence structure in the fair weather trade wind boundary layer. *J. Atmos. Sci.,* **31,** 1308–1323.
Platt, C. M. R., 1997: A parameterization of the visible extinction coefficient of ice clouds in terms of the ice/water content. *J. Atmos. Sci.,* **54,** 2083–2098.
——, S. A. Young, P. J. Manson, G. R. Patterson, S. C. Marsden, R. T. Austin, and J. H. Churnside, 1998: The optical properties of equatorial cirrus from observations in the ARM pilot radiation observation experiment. *J. Atmos. Sci.,* **55,** 1977–1996.
Raymond, D. J., 1995: Regulation of moist convection over the western Pacific warm pool. *J. Atmos. Sci.,* **52,** 3945–3959.
——, and D. J. Torres, 1998: Fundamental moist modes of the equatorial troposphere. *J. Atmos. Sci.,* **55,** 1771–1990.
Redelsperger, J. L., F. Guichard, and M. Sylvain, 2000: A parameterization of mesoscale enhancement of surface fluxes for large-scale models. *J. Climate,* **13,** 402–421.
Rickenbach, T. M., and S. A. Rutledge, 1997: The diurnal variation of rainfall over the western Pacific warm pool: Dependence on convective organization. Preprints, *22d Conf. on Hurricanes and Tropical Meteorology,* Fort Collins, CO, Amer. Meteor. Soc., 205–206.
Rossow, W. B., and R. A. Schiffer, 1991: ISCCP cloud data products. *Bull. Amer. Meteor. Soc.,* **72,** 2–20.
Sarachik, E. S., 1974: The tropical mixed layer and cumulus parameterization. *J. Atmos. Sci.,* **31,** 2222–2225.
Saxen, T. R., and S. A. Rutledge, 1998: Surface fluxes and boundary layer recovery in TOGA COARE: Sensitivity to convective organization. *J. Atmos. Sci.,* **55,** 2763–2781.
Serra, Y. L., D. P. Rogers, D. E. Hagan, C. A. Friehe, R. L. Grossman, R. A. Weller, and S. Anderson, 1997: Atmospheric boundary layer over the central and western equatorial Pacific Ocean observed during COARE and CEPEX. *J. Geophys. Res.,* **102,** 23 217–23 237.
Soloviev, A., and R. Lukas, 1997: Observation of large diurnal warming events in the near-surface layer of the western Pacific warm pool. *Deep-Sea Res.,* **44,** 1055–1076.
Stramma, L., P. Cornillon, R. W. Weller, J. F. Price, and M. G. Briscoe, 1986: Large diurnal sea surface temperature variability: Satellite and in situ measurements. *J. Phys. Oceanogr.,* **16,** 827–837.
Stull, R. B., 1976: The energetics of entrainment across a density interface. *J. Atmos. Sci.,* **33,** 1260–1267.
Sui, C.-H., K.-M. Lau, Y. N. Takayabu, and D. A. Short, 1997a: Diurnal variations in tropical oceanic cumulus convection during TOGA COARE. *J. Atmos. Sci.,* **54,** 639–655.
——, X. Li, K.-M. Lau, and D. Adamec, 1997b: Multiscale air–sea interactions during TOGA COARE. *Mon. Wea. Rev.,* **125,** 448–462.
——, ——, and ——, 1998: Radiative-convective processes in simulated diurnal variations of tropical oceanic convection. *J. Atmos. Sci.,* **55,** 2345–2357.
Sun, J., J. F. Howell, S. K. Esbensen, L. Mahrt, C. M. Greb, R.

Grossman, and M. A. LeMone, 1996: Scale dependence of air–sea fluxes over the western equatorial Pacific. *J. Atmos. Sci.,* **53,** 2997–3012.

Tennekes, H., 1973: A model for the dynamics of the inversion above a convective boundary layer. *J. Atmos. Sci.,* **30,** 558–567.

Velden, C. S., and J. A. Young, 1994: Satellite observations during TOGA COARE: Large-scale descriptive overview. *Mon. Wea. Rev.,* **122,** 2426–2441.

Webster, P. J., 1972: Response of the tropical atmosphere to local steady forcing. *Mon. Wea. Rev.,* **100,** 518–541.

——, and R. Lukas, 1992: TOGA COARE: The Coupled Ocean–Atmosphere Response Experiment. *Bull. Amer. Meteor. Soc.,* **73,** 1377–1416.

——, C. A. Clayson, and J. A. Curry, 1996: Clouds, radiation, and the diurnal cycle of sea surface temperature in the tropical western Pacific. *J. Climate,* **9,** 1712–1730.

Weckwerth, T. M., J. W. Wilson, and R. M. Wakimoto, 1996: Thermodynamic variability within the convective boundary layer due to horizontal convective rolls. *Mon. Wea. Rev.,* **124,** 769–784.

Weller, R. A., and S. P. Anderson, 1996: Surface meteorology and air–sea fluxes in the western equatorial Pacific during the TOGA Coupled Ocean Atmosphere Response Experiment. *J. Climate,* **9,** 1959–1990.

White, A. B., C. W. Fairall, and J. B. Snider, 1995: Surface-based remote sensing of marine boundary-layer cloud properties. *J. Atmos. Sci.,* **52,** 2827–2838.

Williams, A. G., J. M. Hacker, and H. Krans, 1997: Transport processes in the tropical warm pool boundary layer. *J. Atmos. Sci.,* **54,** 2060–2082.

Woolnough, S. J., J. M. Slingo, and B. J. Hoskins, 2000: The relationship between convection and sea surface temperature on intraseasonal timescales. *J. Climate,* **13,** 2086–2104.

Xie, P., and P. A. Arkin, 1997: Global precipitation: A 17-year monthly analysis based on gauge observations, satellite estimates, and numerical model outputs. *Bull. Amer. Meteor. Soc.,* **78,** 2539–2558.

Yin, B., and B. A. Albrecht, 2000: Spatial variability of atmospheric boundary layer structure over the eastern equatorial Pacific. *J. Climate,* **13,** 1574–1592.

Yoneyama, K., and D. B. Parsons, 1999: A proposed mechanism for the intrusion of dry air into the tropical western Pacific region. *J. Atmos. Sci.,* **56,** 1524–1546.

Young, G. S., S. M. Perugini, and C. W. Fairall, 1995: Convective wakes in the equatorial western Pacific during TOGA. *Mon. Wea. Rev.,* **123,** 110–123.

Zhang, C., and M.-D. Chou, 1999: Variability of water vapor, infrared radiative cooling, and atmospheric instability for deep convection in the equatorial western Pacific. *J. Atmos. Sci.,* **56,** 711–723.

——, and M. J. McPhaden, 2000: Intraseasonal surface cooling in the equatorial western Pacific. *J. Climate,* **13,** 2261–2276.

Zipser, E. J., 1977: Mesoscale and convective-scale downdrafts as distinct components of squall-line circulation. *Mon. Wea. Rev.,* **105,** 1568–1589.

——, and R. H. Johnson, 1998: Systematic errors in radiosonde humidities: A global problem? Preprints, *10th Symp. on Meteorological Observations and Instrumentation,* Phoenix, AZ, Amer. Meteor. Soc., 72–73.

Zuidema, P., 1998: On the 600–800-mb minimum in tropical cloudiness. *J. Atmos. Sci.,* **55,** 2220–2228.